scientific reports

OPEN

Design and application of inclined tensioned steel cantilevered scaffolding

Zhihui Zhao[1], Dajiang Geng[2]✉, Yanping Zhang[2], Xiaohuan Wu[3], Enxin Miao[2] & Minjian Long[2]

In order to reduce the cost of scaffolding usage in engineering projects as much as possible under the premise of safety and rationality, while avoiding the risk of leakage caused by holes left in the building structure by the scaffolding, a type of inclined tensioned steel cantilevered scaffolding is proposed based on the stress characteristics of traditional cantilevered scaffolding. Considering the actual construction characteristics, a comprehensive approach involving theoretical analysis, on-site field tests, and finite element methods is adopted to clarify the full-process design method of the inclined tensioned steel cantilevered scaffolding. Additionally, recommendations are provided for the practical engineering design and application of the inclined tensioned steel cantilevered scaffolding. Finally, the inclined tensioned steel cantilevered scaffolding is applied in actual engineering. The research results indicate that the proposed full-process design method is feasible, and the inclined tensioned steel cantilevered scaffolding is more cost-effective than traditional cantilevered scaffolding.

Keywords Inclined tensioned, Full-process design, Overall stress, Node analysis

Scaffolding plays a crucial role in construction, especially in residential building construction. Currently, scaffolding mainly includes forms such as attached lifting platforms, climbing frames, and cantilevered frames, depending on their operational principles. Scholars and engineering professionals worldwide have conducted extensive research on the mechanical mechanisms, load-bearing capacity influencing factors, node performance, and monitoring methods of scaffolding.

The study of mechanical mechanisms primarily employs finite element numerical calculation methods, inductive summarization methods, and experimental methods[1]. The research results of Chen et al.[2] and Wu et al.[3] showed that adding supports and bottom horizontal bars could effectively prevent progressive collapse. El et al.[4] developed the Extensible Arch Steel Truss (EAST) scaffolding system which has higher structural stability and safety factors.

Factors affecting the load-bearing capacity and stability of scaffolding mainly include geometric defects[5–9], various deviations during erection[10], load eccentricity[11], adjacent structures[12], wind loads[13], uneven settlements[14], installation clearances[15], and node connection methods[16–19]. The initial defects in components such as cross braces significantly affect the overall performance of scaffolding[7], and a probability limit state design method for scaffolding considering joint defects can be established based on reliability theory[8]. The mechanical performance of couplers significantly affects the load-bearing capacity and stability of steel pipe coupler scaffolding, with fractures primarily occurring in the bolt connection areas of couplers[16].

There are various forms of scaffold nodes currently, and the study of node performance is mainly conducted through theoretical analysis, numerical calculation, and experimental methods[20–29]. The cyclic loading can cause loosening of the connection nodes, thereby affecting their load-bearing capacity, suggesting the inclusion of relevant considerations in the specifications[20]. The forms of scaffolding nodes include Cuplok system nodes[22], new types of scaffolding nodes[23], wedge-shaped nodes[24,25], plug-in scaffolding nodes[26], circular scaffolding nodes[27], modular scaffolding nodes[28], etc. Nodes can be replaced with various spring models[25] to simplify the analysis of scaffolding forces.

In the process of scaffold usage, monitoring is essential to ensure the safety of engineering construction. Lam et al.[30] applied Internet of Things (IoT) technology to scaffold system fault monitoring, enhancing scaffold safety. IoT and sensor technology enable the monitoring of scaffold abnormalities. Building upon this principle, Lam et al.[31] developed a scaffold safety monitoring and assessment system. Huang et al.[32] conducted real-time

[1]Architectural Engineering Institute, Chongqing Industry Polytechnic College, Chongqing 401120, China. [2]China Construction Fourth Engineering Division Corp. Ltd, Shanghai 201199, China. [3]Transportation Project Management Center of the Central District of Guangzhou, Guangzhou 510145, China. ✉email: gdj1410704@alumni.tongji.edu.cn

comparative analysis using monitored axial forces and lateral displacement data along with computational data, enabling early prediction and control of scaffold system collapses.

A comprehensive review of existing research both domestically and internationally reveals that, despite the application of cantilever scaffolding in engineering, research efforts predominantly focus on construction techniques, with minimal attention given to design methods and design work. However, ensuring construction safety and reliability requires a proactive approach to design. Considering that the cantilever scaffolding can reserve holes in the building structure, causing leakage risks, and the engineering cost is high, in order to reduce the engineering cost and reduce the leakage risk, the inclined steel cantilever scaffolding is proposed. To better guide the design work of inclined steel cantilever scaffolding and improve engineering practice, a comprehensive approach was taken based on previous related work. This involved theoretical analysis, on-site testing, and finite element analysis to conduct overall structural and node force analyses of inclined steel cantilever scaffolding. The result was the establishment of a standard design process for inclined steel cantilever scaffolding, which was subsequently applied to scaffold design for residential construction projects in China.

The main innovation points are as follows: Considering the structural characteristics of traditional cantilever scaffolding, a theory-based analysis method was proposed to develop an inclined steel cantilever scaffolding system. Through a comprehensive approach involving theoretical analysis, on-site tests, and finite element methods, a clear full-process design methodology for the inclined steel cantilever scaffolding was established, providing recommendations for practical engineering design and application of this system. Multivariate analysis methods were employed to specify the key control points in the design and construction process of the inclined steel cantilever scaffolding. By applying the inclined steel cantilever scaffolding and the corresponding full-process design methods in engineering practice, the corresponding economic and social benefits were clarified.

Analysis of the structural characteristics of inclined steel cantilever scaffolding

Comparison with traditional cantilever scaffolding

The differences between inclined steel cantilever scaffolding and traditional cantilever scaffolding are illustrated in Fig. 1. In comparison with traditional cantilever scaffolding, inclined steel cantilever scaffolding offers the following advantages:

(1) Minimal damage to the building structure: Traditional cantilever scaffolding requires openings in shear walls and floor slabs, resulting in significant structural damage. In contrast, inclined steel cantilever scaffolding only requires bolts to be embedded in the outer walls or edge beams, thus causing less damage to the structure.

(2) High material utilization efficiency and cost-effectiveness: The uneven distribution of internal forces in the main beams of traditional cantilever scaffolding results in a higher degree of variability in the mechanical performance of steel main beams at different locations, leading to inefficient material utilization. In contrast, the degree of variability in the mechanical performance of the main steel beams of inclined steel cantilever scaffolding is relatively small. Furthermore, inclined steel cantilever scaffolding can save more than

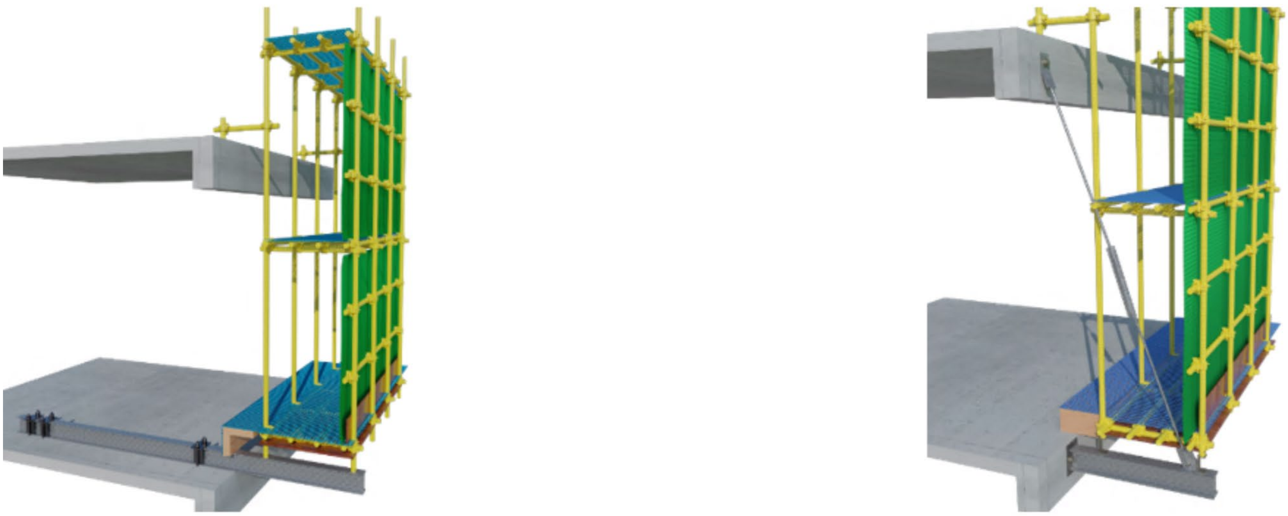

(a) (b)

Fig. 1. Comparison of two types of scaffolding. (**a**) Traditional cantilever scaffolding; (**b**) inclined steel cantilever scaffolding.

50% of the steel consumption compared to traditional cantilever scaffolding, resulting in higher material utilization efficiency and better cost-effectiveness.

(3) Convenient construction, time-saving: The anchoring segment of the main steel beams of traditional cantilever scaffolding extends into the interior by 1.25 times the cantilever segment length, requiring openings in both floor slabs and walls, leading to a complex construction process. Additionally, sealing and dismantling of the steel beams are required later, increasing construction difficulty. In contrast, inclined steel cantilever scaffolding mainly adopts prefabrication, resulting in a relatively faster construction speed. Moreover, inclined steel cantilever scaffolding does not require anchoring segments indoors, thus not affecting the construction of interior masonry and floor projects.

(4) Reduced risk of leakage: Traditional cantilever scaffolding requires openings in floor slabs and walls, while inclined steel cantilever scaffolding only requires bolt embedment in outer walls or edge beams. Clearly, sealing is required for all openings created by traditional cantilever scaffolding, whereas only minor sealing work is needed for inclined steel cantilever scaffolding, significantly reducing construction workload and the risk of structural leakage.

Composition of inclined steel cantilever scaffolding

In comparison with traditional cantilever scaffolding, inclined steel cantilever scaffolding consists not only of footboards, longitudinal horizontal bars, transverse horizontal bars, uprights, guardrails, and couplers but also primarily of tie rods and main beams, as depicted in Fig. 2a. The tie rods and main beams constitute the main load-bearing structure. Additionally, inclined steel cantilever scaffolding includes four major nodes: the connection nodes between the main beam and the building structure (Fig. 2b), the connection nodes between the tie rods and the main beam (Fig. 2c), the upper and lower connection nodes of the tie rods (Fig. 2d), and the connection nodes between the tie rods and the building structure (Fig. 2e). The scaffolding's load is mainly transmitted from the uprights to the main beams, then to the tie rods, and finally to the four major nodes.

Analysis of overall force on inclined steel cantilever scaffolding

By comparing Fig. 1a,b, it can be observed that the steel pipe scaffolding part of the inclined steel cantilever scaffolding is identical to that of traditional cantilever scaffolding. Therefore, the force analysis of the corresponding steel pipe scaffolding part of the inclined steel cantilever scaffolding can refer to the force analysis of the corresponding part of traditional cantilever scaffolding, mainly including the strength and stability of longitudinal horizontal bars, transverse horizontal bars, uprights, ledger stability, and calculation of coupler anti-slip forces[33]. Unlike traditional cantilever scaffolding, which only consists of cantilever beams, the inclined steel cantilever scaffolding includes cantilever main beams and tie rods, as shown in Fig. 3. The structural force analysis should focus on the overall force of the cantilever main beams and tie rods.

As shown in Fig. 3, the force situation of the structure composed of cantilever main beams and tie rods is analyzed. The analysis assumes that the upper end of the tie rod is hinged, and the left side of the cantilever main beam is fixed. Considering that the situation of two tie rods is commonly applied in engineering, and one tie rod is just a special case of two tie rods, an analysis of the situation with two tie rods is conducted. In addition, theoretically, the tie rod and the cantilever main beam should be located in the same vertical plane, and the upper hinge point of the tie rod and the left fixed point of the cantilever main beam should be located on the same vertical line. However, in practical engineering, due to various site conditions, it is highly likely that there will be deviations in the nodes where the tie rod is connected to the structure, resulting in the tie rod and the main beam not being in the same vertical plane. The architectural structural form can cause the upper hinge point of the tie rod and the left fixed point of the cantilever main beam not to be located on the same vertical line. Let the offset of the tie rod upper node as shown in the figure be denoted as t_0 and the horizontal distance between the left fixed point of the cantilever main beam and the upper node of the tie rod, projected lengthwise along the axial direction of the cantilever main beam, be denoted as l_0.

The cantilever main beam mainly bears the concentrated load transmitted by the uprights, denoted as load F_{n} and the uniformly distributed self-weight load, denoted as load q. The structure composed of the cantilever main beam and tie rods is a hyperstatic structure, where the cantilever main beam sustains bidirectional bending, axial compression, and shear forces, while the tie rods endure axial tensile forces. Based on the force equilibrium at the connection points between the tie rods and the main beam, as well as the vertical displacement coordination, the tension forces in the two tie rods can be easily determined

$$F_{\mathrm{pri}} = \frac{\mathit{\Psi}_{\mathrm{i}}\mathit{\Xi}_{\mathrm{o}} - \mathit{\Omega}_{\mathrm{o}}\mathit{\Psi}_{\mathrm{o}}}{\mathit{\Xi}_{\mathrm{i}}\mathit{\Xi}_{\mathrm{o}} - \mathit{\Omega}_{\mathrm{i}}\mathit{\Omega}_{\mathrm{o}}} \tag{1}$$

and

$$F_{\mathrm{pro}} = \frac{\mathit{\Xi}_{\mathrm{i}}\mathit{\Psi}_{\mathrm{o}} - \mathit{\Omega}_{\mathrm{i}}\mathit{\Psi}_{\mathrm{i}}}{\mathit{\Xi}_{\mathrm{i}}\mathit{\Xi}_{\mathrm{o}} - \mathit{\Omega}_{\mathrm{i}}\mathit{\Omega}_{\mathrm{o}}} \tag{2}$$

where, the process variables $\mathit{\Omega}_{\mathrm{i}}$, $\mathit{\Omega}_{\mathrm{o}}$, $\mathit{\Xi}_{\mathrm{i}}$, $\mathit{\Xi}_{\mathrm{o}}$, $\mathit{\Psi}_{\mathrm{i}}$, and $\mathit{\Psi}_{\mathrm{o}}$ represent

$$\mathit{\Omega}_{\mathrm{i}} = 4\sin(\theta_{\mathrm{i}}){l_{\mathrm{ppi}}}^2(3l_{\mathrm{ppo}} - l_{\mathrm{ppi}}) \tag{3}$$

$$\mathit{\Omega}_{\mathrm{o}} = 4\sin(\theta_{o}){l_{\mathrm{ppi}}}^2(3l_{\mathrm{ppo}} - l_{\mathrm{ppi}}) \tag{4}$$

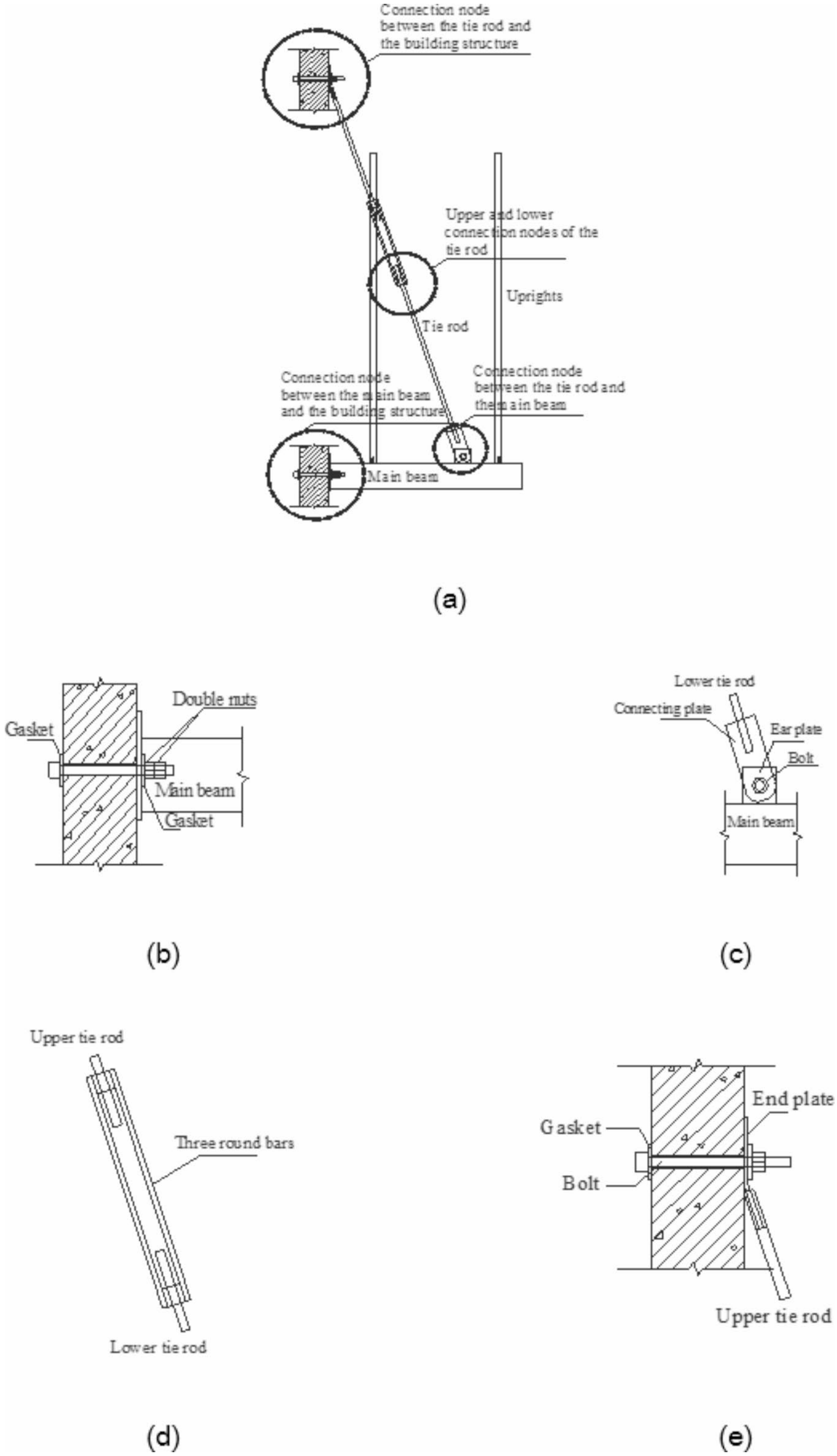

Fig. 2. Composition of inclined steel cantilever scaffolding: (**a**) overall structure; (**b**) connection nodes between main beam and building structure; (**c**) connection nodes between tie rod and main beam; (**d**) upper and lower connection nodes of tie rod; (**e**) connection nodes between tie rod and building structure.

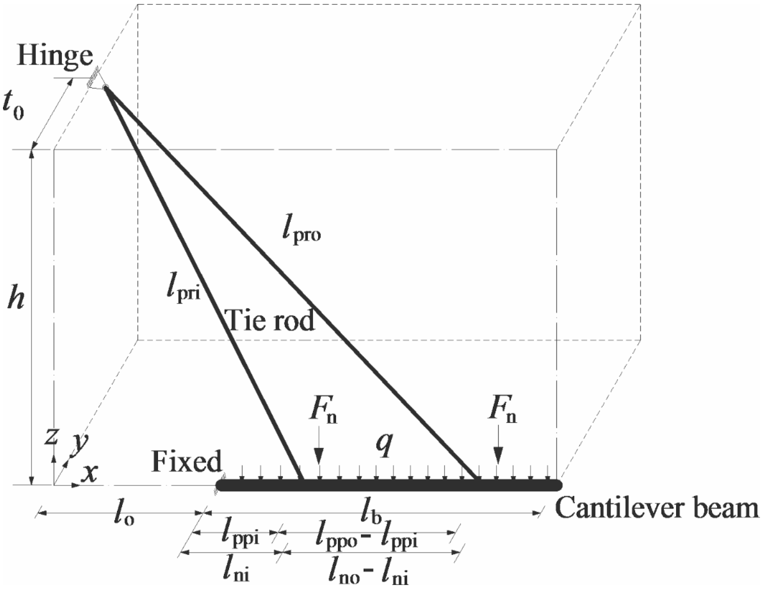

Fig. 3. Overall force diagram.

$$\Xi_{\mathrm{i}} = \frac{24E_b I_y h}{E_{\mathrm{pri}} A_{\mathrm{pri}}} + 8\sin(\theta_{\mathrm{i}}) {l_{\mathrm{ppi}}}^3 \tag{5}$$

$$\Xi_{\mathrm{o}} = \frac{24E_b I_y h}{E_{\mathrm{pro}} A_{\mathrm{pro}}} + 8\sin(\theta_o) {l_{\mathrm{ppo}}}^3 \tag{6}$$

$$\Psi_{\mathrm{i}} = 4F_{\mathrm{n}} {l_{\mathrm{ppi}}}^2 (3l_{\mathrm{ni}} - l_{\mathrm{ppi}}) + 4F_{\mathrm{n}} {l_{\mathrm{ppi}}}^2 (3l_{\mathrm{no}} - l_{\mathrm{ppi}}) + q {l_{\mathrm{ppi}}}^2 ({l_{\mathrm{ppi}}}^2 + 6{l_{\mathrm{b}}}^2 - 4l_{\mathrm{b}} l_{\mathrm{ppi}}) \tag{7}$$

$$\Psi_{\mathrm{o}} = 4F_{\mathrm{n}} {l_{\mathrm{ni}}}^2 (3l_{\mathrm{ppo}} - l_{\mathrm{ni}}) + 4F_{\mathrm{n}} {l_{\mathrm{ppo}}}^2 (3l_{\mathrm{no}} - l_{\mathrm{ppo}}) + q {l_{\mathrm{ppo}}}^2 ({l_{\mathrm{ppo}}}^2 + 6{l_{\mathrm{b}}}^2 - 4l_{\mathrm{b}} l_{\mathrm{ppo}}) \tag{8}$$

θ_{i} and θ_o each satisfy

$$\tan(\theta_{\mathrm{i}}) = \frac{h}{\sqrt{(t_0)^2 + (l_0 + l_{\mathrm{ppi}})^2}} \tag{9}$$

$$\tan(\theta_{\mathrm{o}}) = \frac{h}{\sqrt{(t_0)^2 + (l_0 + l_{\mathrm{pp0}})^2}} \tag{10}$$

As shown in Fig. 3, h denotes the vertical distance between the upper node of the tie rod and the fixed point on the main beam; l_{ppi} and l_{ppo} respectively represent the horizontal distances from the connection nodes of the inner and outer tie rods to the fixed point on the main beam; E_b represents the elastic modulus of the main beam; I_y denotes the moment of inertia of the main beam about the axis y; E_{pri} and E_{pro} respectively represent the elastic moduli of the inner and outer tie rods; A_{pri} and A_{pro} respectively denote the cross-sectional areas of the inner and outer tie rods; l_{ni} and l_{no} respectively represent the horizontal distances from the points of application of the inner and outer concentrated loads F_{n} to the fixed point on the main beam; l_{b} represents the length of the main beam.

The bending moment of the cantilevered main beam is

$$M_{\mathrm{y}} = \begin{cases} \left(\frac{1}{2}q(l_{\mathrm{b}} - x)^2 + F_{\mathrm{n}}(l_{\mathrm{ni}} + l_{\mathrm{no}} - 2x) - F_{\mathrm{pri}}\sin(\theta_i)(l_{\mathrm{ppi}} - x) - F_{\mathrm{pro}}\sin(\theta_o)(l_{\mathrm{ppo}} - x)\right) & 0 \le x < l_{\mathrm{ppi}} \\ \left(\frac{1}{2}q(l_{\mathrm{b}} - x)^2 + F_{\mathrm{n}}(l_{\mathrm{ni}} + l_{\mathrm{no}} - 2x) - F_{\mathrm{pro}}\sin(\theta_o)(l_{\mathrm{ppo}} - x)\right) & l_{\mathrm{ppi}} \le x < l_{\mathrm{ni}} \\ \left(\frac{1}{2}q(l_{\mathrm{b}} - x)^2 + F_{\mathrm{n}}(l_{\mathrm{no}} - x) - F_{\mathrm{pro}}\sin(\theta_{\mathrm{o}})(l_{\mathrm{ppo}} - x)\right) & l_{\mathrm{ni}} \le x < l_{\mathrm{ppo}} \\ \left(\frac{1}{2}q(l_{\mathrm{b}} - x)^2 + F_{\mathrm{n}}(l_{\mathrm{no}} - x)\right) & l_{\mathrm{ppo}} \le x < l_{\mathrm{no}} \\ \frac{1}{2}q(l_{\mathrm{b}} - x)^2 & l_{\mathrm{no}} \le x \le l_{\mathrm{b}} \end{cases} \tag{11}$$

and

$$M_z = \begin{cases} \left(F_{\mathrm{pri}}\frac{t_0}{l_{\mathrm{pri}}}(l_{\mathrm{ppi}} - x) + F_{\mathrm{pro}}\frac{t_0}{l_{\mathrm{pro}}}(l_{ppo} - x)\right) & 0 \le x < l_{ppi} \\ \left(F_{pro}\frac{t_0}{l_{pro}}(l_{ppo} - x)\right) & l_{ppi} \le x < l_{ppo} \\ 0 & l_{ppo} \le x \le l_b \end{cases} \tag{12}$$

Here, M_{y} and M_{z} respectively represent the bending moments of the main beam about the *y*-axis and the *z*-axis.

Taking the horizontal distance *x* from the fixed end of the cantilevered main beam as the variable, differentiating Eqs. (11) and (12), the shear force of the cantilevered main beam can be readily obtained

$$V_z = \begin{cases} (-q(l_{\mathrm{b}} - x) - 2F_{\mathrm{n}} + F_{\mathrm{pri}}\sin(\theta_i) + F_{\mathrm{pro}}\sin(\theta_o)) & 0 \le x < l_{\mathrm{ppi}} \\ (-q(l_{\mathrm{b}} - x) - 2F_{\mathrm{n}} + F_{\mathrm{pro}}\sin(\theta_o)) & l_{\mathrm{ppi}} \le x < l_{\mathrm{ni}} \\ (-q(l_{\mathrm{b}} - x) - F_{\mathrm{n}} + F_{\mathrm{pro}}\sin(\theta_o)) & l_{\mathrm{ni}} \le x < l_{\mathrm{ppo}} \\ -q(l_{\mathrm{b}} - x) - F_{\mathrm{n}} & l_{\mathrm{ppo}} \le x < l_{\mathrm{no}} \\ -q(l_{\mathrm{b}} - x) & l_{\mathrm{no}} \le x \le l_{\mathrm{b}} \end{cases} \tag{13}$$

and

$$V_y = \begin{cases} -F_{\mathrm{pri}}\frac{t_0}{l_{\mathrm{pri}}} - F_{\mathrm{pro}}\frac{t_0}{l_{\mathrm{pro}}} & 0 \le x < l_{\mathrm{ppi}} \\ -F_{\mathrm{pro}}\frac{t_0}{l_{\mathrm{pro}}} & l_{\mathrm{ppi}} \le x < l_{\mathrm{ppo}} \\ 0 & l_{\mathrm{ppo}} \le x \le l_{\mathrm{b}} \end{cases} \tag{14}$$

The axial force of the cantilevered main beam is

$$N_x = \begin{cases} -F_{\mathrm{pri}}\frac{l_0 + l_{\mathrm{ppi}}}{l_{\mathrm{pri}}} - F_{\mathrm{pro}}\frac{l_0 + l_{\mathrm{ppo}}}{l_{\mathrm{pro}}} & 0 \le x < l_{\mathrm{ppi}} \\ -F_{\mathrm{pro}}\frac{l_0 + l_{\mathrm{ppo}}}{l_{\mathrm{pro}}} & l_{\mathrm{ppi}} \le x < l_{\mathrm{ppo}} \\ 0 & l_{\mathrm{ppo}} \le x \le l_{\mathrm{b}} \end{cases} \tag{15}$$

Specifically, tensile axial force is considered positive, while compressive axial force is negative.

The maximum deflection of the cantilevered main beam occurs at the free end of the beam and is given by

$$\begin{aligned} w\max = &-\frac{F_{\mathrm{pri}}\sin(\theta_{\mathrm{i}}){l_{\mathrm{ppi}}}^2}{6E_bI_y}(3l_{\mathrm{b}} - l_{\mathrm{ppi}}) - \frac{F_{\mathrm{pro}}\sin(\theta_o){l_{\mathrm{ppo}}}^2}{6E_bI_y}(3l_{\mathrm{b}} - l_{\mathrm{ppo}}) \\ &+ \frac{F_{\mathrm{n}}{l_{\mathrm{ni}}}^2}{6E_bI_y}(3l_{\mathrm{b}} - l_{\mathrm{ni}}) + \frac{F_{\mathrm{n}}{l_{\mathrm{no}}}^2}{6E_bI_y}(3l_{\mathrm{b}} - l_{\mathrm{no}}) + \frac{q{l_{\mathrm{b}}}^4}{8E_bI_y} \end{aligned} \tag{16}$$

Overall design calculation

The stress states of the cantilevered scaffolding with inclined steel beams are different during the installation process, normal usage, and dismantling process, mainly reflected in whether the tie rods are in action and the variation of the concentrated load F_{n} transmitted from the vertical poles to the cantilevered main beam.

Installation process

During the installation process of the inclined steel beam cantilevered scaffolding, the cantilevered main beam is first installed, followed by the installation of the tie rods. Throughout the entire installation process, the most critical moment occurs when the cantilevered main beam installation is completed while the tie rods are being installed but not yet in effect. At this point, the cantilevered main beam is supported by the vertical poles of the lower scaffolding, which provide support to the cantilevered main beam. Only after the tie rods are fully installed and in effect will the vertical poles of the lower scaffolding be removed. Conversely, during the dismantling process, the most critical state corresponds to when the tie rods are just removed. At this point, the tie rods are no longer in effect, and there are no supporting vertical poles beneath the lower part of the cantilevered main beam, which is firmly attached to the building structure. Clearly, the stress conditions during the dismantling process are more unfavorable than during the installation process, thus requiring a focused calculation on the dismantling process.

Normal usage

In the case of normal usage, when all construction loads are applied to the cantilever beam through the uprights, the cantilever beam and tie rod system experience the maximum load. It is necessary to conduct a stress analysis on the cantilever beam and tie rod at this point to clarify their respective load states.

The cantilever beam requires strength, deflection, and stability verification. During strength verification, considering the offset of the node where the tie rod connects to the structure (i.e., $t_0 \neq 0$), the cantilever beam experiences bidirectional bending, bidirectional shear, and axial pressure simultaneously. It is recommended to verify this using the sectional strength calculation formula for compression-bending members within two principal planes as specified in the relevant code[34]. Specifically, the axial force used in the calculation process should follow Eq. (15), while the bidirectional bending moments should be calculated separately using Eqs. (11) and (12). Additionally, verification of shear strength for the actual web components subjected to bending in the principal planes is required. When not considering the offset of the node where the tie rod connects to the structure (i.e., $t_0 = 0$), the cantilever beam experiences unidirectional bending, unidirectional shear force, and axial pressure simultaneously. It is advisable to still utilize the sectional strength calculation formula for compression-bending members within two principal planes as specified in the relevant code[34], with the value of the other bending moment kept constant at zero. Verification of shear strength can still be conducted following the method for web components subjected to bending in the principal planes.

Deflection calculation for the cantilever beam can be performed using Eq. (16), and the calculated deflection should meet the allowable deflection values specified in the relevant code[34].

Stability verification needs to consider both overall stability and local stability. Overall stability can be verified using the method specified in the relevant code[34] for the overall stability of double-axis symmetric solid web section compression-bending members within two principal planes, with the value of the other bending moment kept constant at zero. Local stability can be verified based on the width-to-thickness ratio of the belly plate of compression-bending members as specified in the relevant code[34].

For tie rods, only strength verification is necessary, ensuring that the actual tension force calculated according to Eqs. (1) and (2), divided by the corresponding cross-sectional area of the tie rod, does not exceed the allowable tension stress.

Dismantling process

During the dismantling process, when the tie rods are first removed, most of the construction steel pipe scaffolding has already been dismantled. Only a portion of the construction load is transmitted to the cantilever beam through the uprights at this point, and the tie rods no longer play a role while the lower part of the cantilever beam is also unsupported. The cantilever beam can then be simplified as a cantilever beam subjected to unidirectional bending and unidirectional shear simultaneously. In specific calculations, the moments, shear forces, and maximum deflection of the cantilever beam can be determined using Eqs. (11), (13), and (16) respectively. Similarly, strength, deflection, and stability verification are required for the cantilever beam.

During strength verification, when the cantilever beam is subjected to unidirectional bending and unidirectional shear, it is recommended to perform bending strength and shear strength verification following the method for web components subjected to bending in the principal planes as specified in the relevant code[34]. For deflection verification, the calculated deflection should meet the allowable deflection values specified in the relevant code[34]. Overall stability verification can be conducted using the formula for the overall stability of bending members subjected to maximum stiffness within the principal planes as specified in the relevant code[34].

Considering the relatively simple design of the tie rods, only strength verification during the normal usage phase is necessary. However, the cantilever beam requires staged strength, deflection, and stability verification. The comprehensive design process for the cantilever beam is summarized in Table 1 for reference in practical engineering design work.

Case study of whole process design calculation

The summary of the cantilever main beam verification for the process design, as shown in Table 1, indicates that verification is only required for normal usage and dismantling processes. The parameter values used in the calculations are presented in Table 2. During normal usage, all rods are fully functional, with a concentrated load design value of $F_{\mathrm{n}} = 10.14\ \mathrm{kN}$; during dismantling, all rods are ineffective, with a concentrated load design value of $F_{\mathrm{n}} = 1.69\ \mathrm{kN}$. The comparison of the moments, shear forces, and axial forces of the main beam between the normal usage and dismantling stages, calculated according to Eqs. (11), (13), and (15), respectively, are illustrated in Fig. 4a–c. From the figures, it is evident that the bending resistance requirement for the main beam during dismantling exceeds that of the normal usage stage, while the shear resistance requirement during dismantling is lower than that of the normal usage stage. When assessing the shear carrying capacity of the left fixed node of the main beam, the shear force calculation results corresponding to the dismantling stage should be utilized. The compressive resistance requirement for the main beam during dismantling is lower than that of the normal usage stage.

According to Eq. (16), the maximum deflections of the main beam during normal usage and dismantling phases are calculated as 0.9904 mm and 3.1624 mm, respectively. It can be observed that the requirements for deflection and deformation resistance are lower during the normal usage phase compared to the dismantling phase, primarily due to the significant contribution of the two rods. Therefore, it is recommended that subsequent main beam design work and the verification of main beam fixed joint nodes must simultaneously consider the loading conditions during both normal usage and dismantling phases.

Verification stage	Tie rod effectiveness	Support at bottom of main beam	Concentrated load	Section stress verification	Strength verification	Deflection verification	Stability verification
Installation	No	Yes	Partial	–	–	–	–
Normal usage	Yes	No	All	Biaxial bending + Biaxial bhear + Axial compression	Biaxial bending member section strength + Shear strength of members bending in principal planes	Deflection of bending members	Overall stability + Local stability
Dismantling	No	No	Partial	Unidirectional bending + Unidirectional shear	Bending strength and shear strength of members bending in principal planes	Deflection of bending members	Overall stability

Table 1. Summary of cantilever beam verification in full process design.

Parameter	Value	Parameter	Value
h (m)	3.00	t_0	0.00 h
l_b (m)	2.10	l_0	0.00 h
l_{ni} (m)	1.15	l_{ppi}	0.90 l_{ni}
l_{no} (m)	2.00	l_{ppo}	0.90 l_{no}
Section of I-beam	I16	E_b (kN/m^2)	2.06×10^8
Diameter of inner rod d_{pri} (mm)	20	E_{pri} (kN/m^2)	2.06×10^8
Diameter of outer rod d_{pro} (mm)	20	E_{pro} (kN/m^2)	2.06×10^8

Table 2. Parameter value table of whole process design.

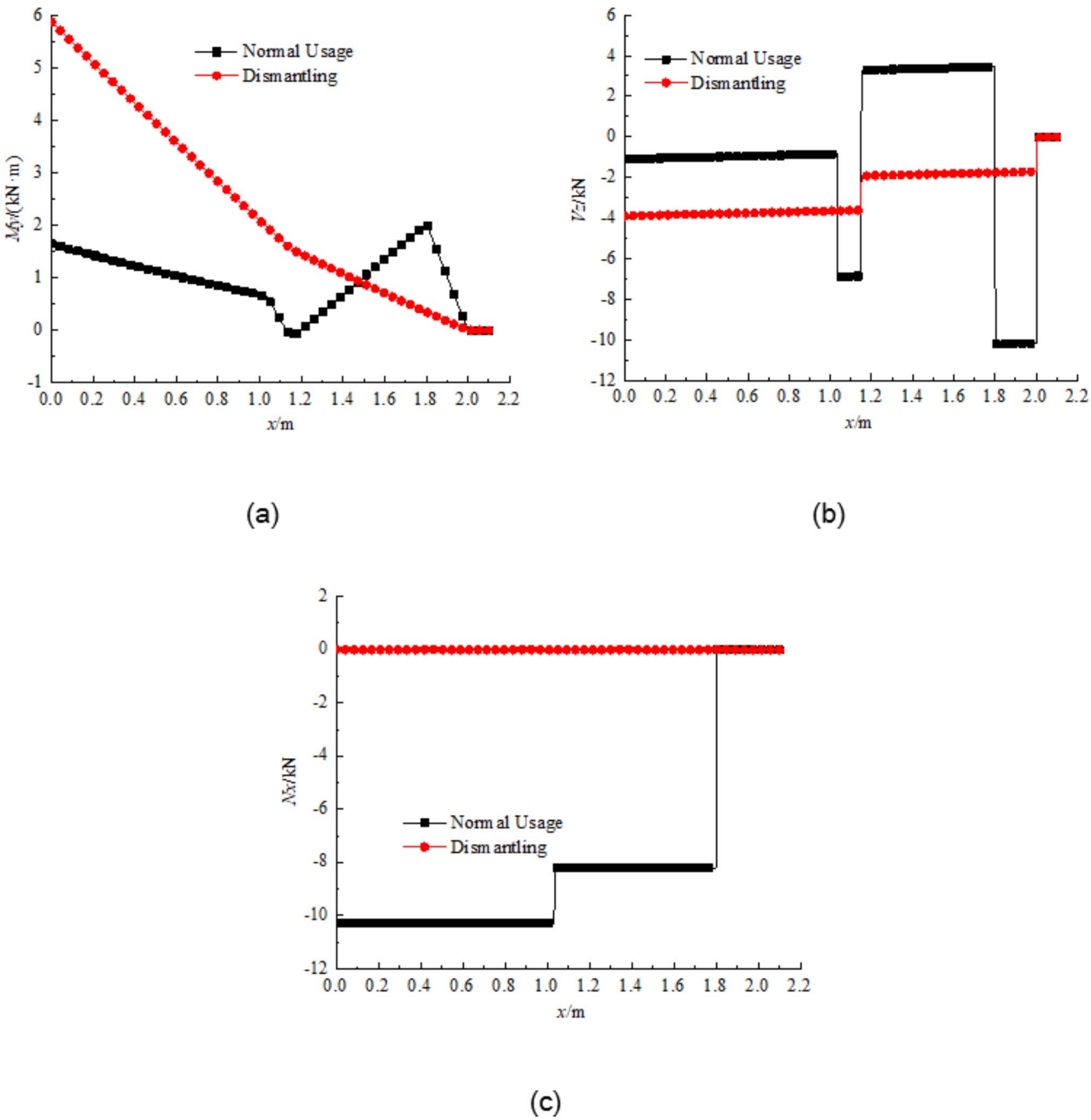

Fig. 4. Comparison of internal forces in the main beam between normal usage phase and dismantling phase: (**a**) bending moment M_y; (**b**) shear force V_z; (**c**) Axial force N_x.

Analysis of the force mechanism of suspended steel cantilever scaffolding under several special conditions

Description of special conditions

Ideally, the tension rod and the main beam would be positioned within the same vertical plane, i.e., $t_0 = 0$, and the upper hinge point of the tension rod would align with the left fixed point of the cantilever main beam on the same vertical line, i.e., $l_0 = 0$. However, various situations inevitably arise in practical engineering. Therefore, a summary of the possible conditions encountered in various engineering scenarios is presented in Table 3.

From Table 3, it is evident that the occurrence of any one of three conditions - the failure of bolts at the connection points between the tension rod and the building structure, the failure of bolts at the connection points between the tension rod and the main beam, and excessive length of the tension rod can lead to the corresponding failure of the tension rod. Thus, in the calculation, it is necessary to consider $A_{\text{pri}} = 0$ or $A_{\text{pro}} = 0$. The failure of bolts at the connection point between the main beam and the building structure, as well as the hanging of the uprights, results in the inability of the load of the steel pipe scaffold to be transmitted to the analyzed cantilever main beam through the uprights, but only to the adjacent two main beams, causing the vertical load borne by the adjacent two main beams transmitted by the uprights, denoted as F_{n}, to increase by 1.5 times.

Analysis of calculation examples for special working conditions

(1) Node offset on tension rod.

Node offset on the tension rod, denoted as $t_0 \neq 0$, is analyzed with t_0 set to 0.00 *h*, 0.05 *h*, 0.10 *h*, and 0.15 *h*, resulting in four scenarios. The calculation results are presented in Fig. 5. From the Fig. 5, it is evident that the influence of node offset on the bending moment M_{y}, shear force V_{z}, and axial force N_{x} along the strong axis direction is minimal. However, significant increases are observed in bending moment M_{z} and shear force V_y along the weak axis direction as the offset increases. The occurrence of rod offset transforms the uniaxial bending and shearing of the main beam into biaxial bending and shearing, which is highly detrimental to the stress distribution within the main beam and its fixed joint nodes. Additionally, bending moment M_{z} and shear force V_y along the weak axis direction reach their maximum values at the fixed joint end of the main beam, thereby increasing the stress on the fixed joint nodes. Therefore, node offset on the tension rod is unfavorable for both the stress distribution within the main beam itself and the stress on the fixed joint nodes. In the four scenarios, the maximum deflection of the main beam is calculated as 0.9904 mm, 0.9912 mm, 0.9937 mm, and 0.9977 mm, respectively, indicating that node offset has minimal impact on the maximum deflection of the main beam.

When t_0 is set to 0.00 *h*, 0.05 *h*, 0.10 *h*, and 0.15 *h*, the corresponding axial forces in the tension rods are 6.3918 kN, 6.3980 kN, 6.4164 kN, and 6.4470 kN, respectively, for the inner tension rod, and 15.9290 kN, 15.9432 kN, 15.9855 kN, and 16.0559 kN, respectively, for the outer tension rod. The axial force along the bolt axis at the node on the tension rod is 10.2800 kN, 10.2795 kN, 10.2778 kN, and 10.2749 kN, respectively. The shear force along the bolt tangential to the node on the tension rod is 19.7013 kN, 19.7246 kN, 19.7942 kN, and 19.9097 kN, respectively. It can be seen that the offset of the node on the tension rod has little effect on the tension rod itself and the forces at the node on the tension rod.

In summary, the offset of the node on the tension rod will have an adverse effect on the main beam and the fixed connection nodes of the main beam. It is recommended to avoid tension rod offset as much as possible during actual construction. If unavoidable, it is suggested to establish two sets of tension rod systems with the vertical plane where the main beam is located as the symmetrical plane.

(2) Bolt failure at the connection point between tension rod and building structure or bolt failure at the connection point between tension rod and main beam or overlong tension rod.

Bolt failure at the connection point between the tension rod and the building structure or Bolt failure at the connection point between the tension rod and the main beam, or an overlong tension rod, occurs when

Conditions	Treatment
Node offset on tension rod	$t_0 \neq 0$, actual values should be considered.
Bolt failure at the connection point between tension rod and building structure	The cross-sectional area of the corresponding tension rod is considered as 0, i.e., $A_{\text{pri}} = 0$ or $A_{\text{pro}} = 0$.
Bolt failure at the connection point between tension rod and main beam	The cross-sectional area of the corresponding tension rod is considered as 0, i.e., $A_{\text{pri}} = 0$ or $A_{\text{pro}} = 0$.
Bolt failure at the connection point between main beam and building structure	Both the main beam and the tension rod fail simultaneously, and the concentrated load F_{n} borne by the adjacent main beam becomes $1.5F_{\text{n}}$.
Excessive length of tension rod	The cross-sectional area of the corresponding tension rod is considered as 0, i.e., $A_{\text{pri}} = 0$ or $A_{\text{pro}} = 0$.
Hanging of uprights	$F_{\text{n}} = 0$ at the corresponding position, and the concentrated load F_{n} borne by the adjacent main beam becomes $1.5F_{\text{n}}$.
Right-angle corner of building structure	In addition to bearing the concentrated load F_{n} and the uniformly distributed self-weight load *q* transmitted by the uprights, the cantilever main beam also needs to bear the concentrated load transmitted by the corresponding secondary beams. A comprehensive force analysis of the structural system composed of the cantilever main beam and tension rod needs to be conducted again.
Encroachment of building structure	$l_0 \neq 0$, actual values should be considered.

Table 3. Several special working conditions and calculation methods.

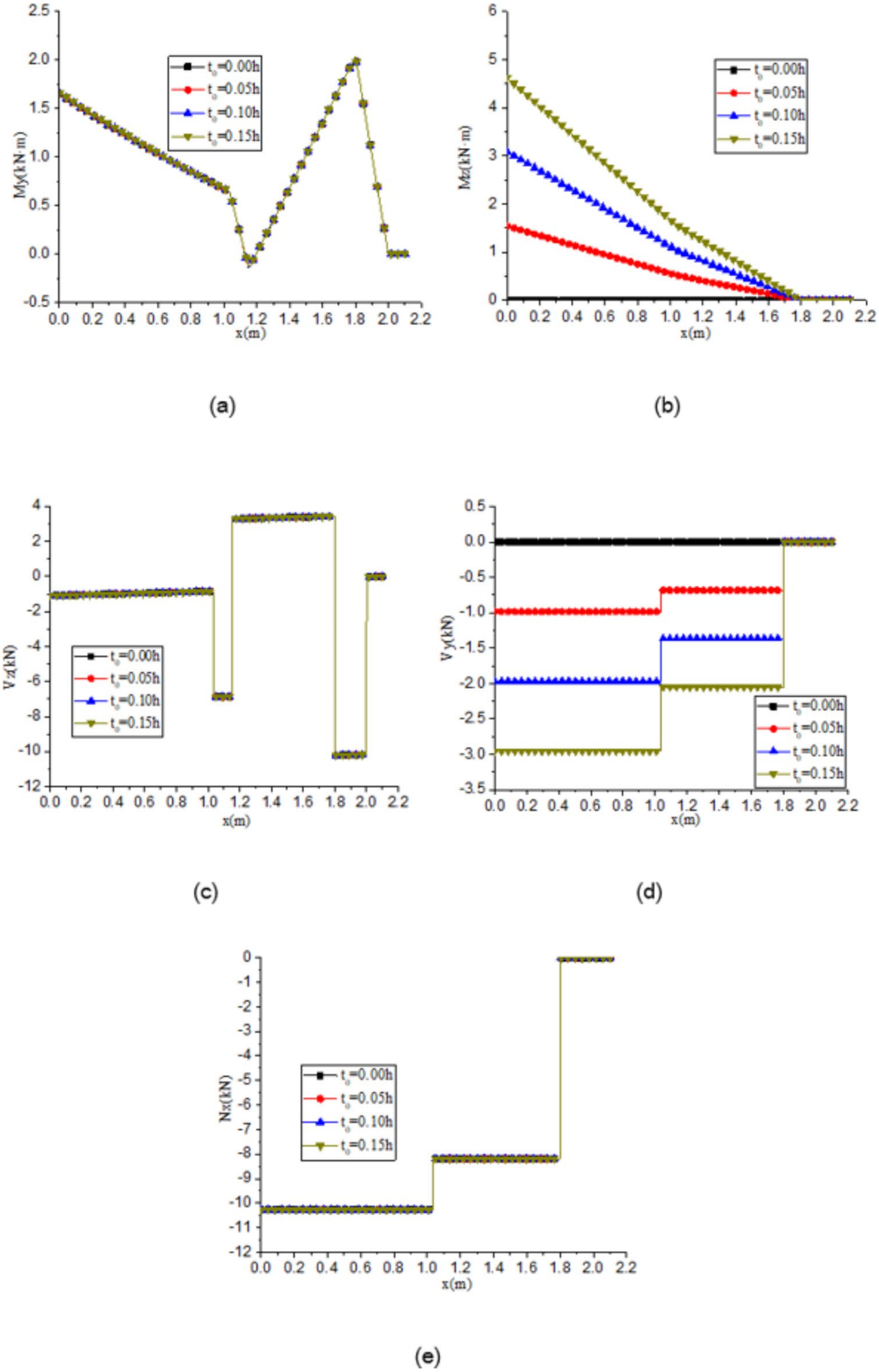

Fig. 5. Comparison of calculation results for node offset on tension rod: (**a**) bending moment M_{y}; (**b**) bending moment M_{z}; (**c**) shear force V_{z}; (**d**) shear force V_y; (**e**) axial force N_{x}.

$A_{\mathrm{pri}} = 0$ or $A_{\mathrm{pro}} = 0$. By setting $A_{\mathrm{pri}} \neq 0$ and $A_{\mathrm{pro}} \neq 0$, $A_{\mathrm{pri}} = 0$ and $A_{\mathrm{pro}} \neq 0$, $A_{\mathrm{pri}} \neq 0$ and $A_{\mathrm{pro}} = 0$, $A_{\mathrm{pri}} = 0$ and $A_{\mathrm{pro}} = 0$ respectively, the calculation results shown in Fig. 6 are obtained.

From the calculation results shown in Fig. 6, it can be observed that there is little difference in the internal force diagram of the main beam between the cases where the inner tension rod fails and when it does not fail. This indicates that the effect of the inner tension rod is limited in the presence of the outer tension rod. A comparison of the internal force diagrams of the main beam under the scenarios of only the inner tension rod

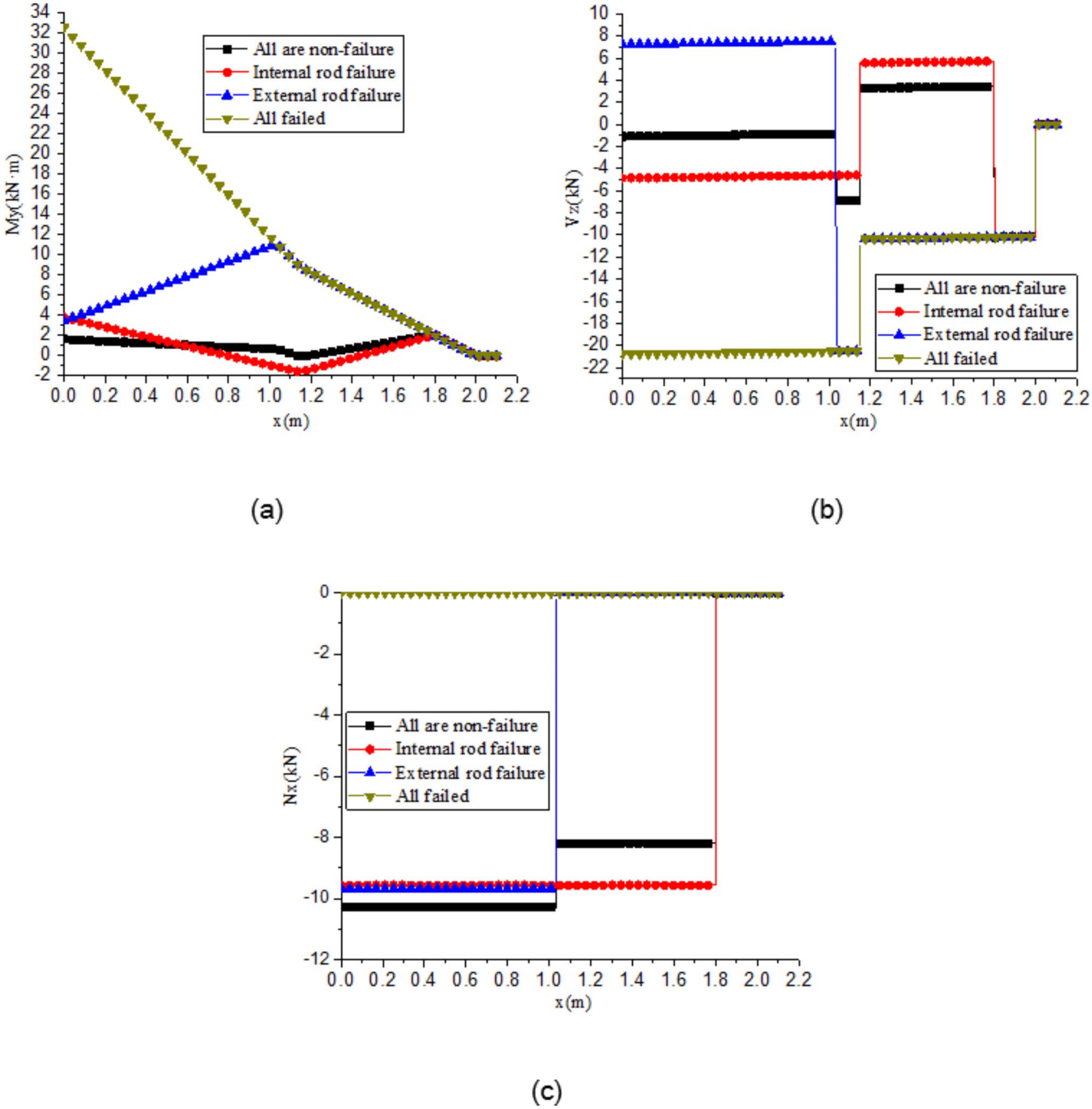

Fig. 6. Comparison of calculation results for rod failure conditions: (**a**) bending moment M_y; (**b**) shear force V_z; (**c**) axial force N_x.

failing and only the outer tension rod failing reveals that the effect of the outer tension rod is much greater than that of the inner tension rod. When both tension rods fail, the bending moment and shear force on the main beam increase significantly, which is highly unfavorable for both the main beam itself and its fixed connection nodes. It is recommended that in actual design work, the outer tension rod must be set when tension rods are installed, as it plays a larger role compared to the inner tension rod. The most ideal situation is to set both inner and outer tension rods simultaneously to minimize the internal forces on the main beam. It is also suggested to regularly inspect the tension rods, especially the outer ones, during the actual use of scaffolding to ensure their effectiveness.

(3) Bolt failure at the connection point between main beam and building structure or unsupported upright.

Bolt failure at the connection point between the main beam and the building structure or an unsupported upright results in a condition where $F_n = 0$ for the corresponding main beam, while the adjacent main beam has its F_n value increased by a factor of 1.5. Therefore, calculations are performed with F_n taken as 0.00 times, 1.00 times, and 1.50 times of the original value to clarify the effect of this condition on the scaffolding load. The comparison of calculation results is presented in Table 4, where M_y represents the maximum bending moment

Variation of F_{n}	M_{y}, maximum value (kN m)	V_{z}, maximum value (kN)	Shear force at fixed end (kN)	$w_{\max}$ (mm)	F_{pri} (kN)	F_{pro} (kN)
0.00	0.0754	− 0.2024	− 0.2024	0.0113	0.1364	0.2164
1.00	2.0380	− 10.2134	− 1.0956	0.9904	6.3918	15.9290
1.50	3.0515	− 15.2834	− 1.5422	1.4800	9.5195	23.7854

Table 4. Comparison of calculation results under different values of F_{n}.

l_0/h	M_{y}, maximum value (kN m)	V_{z}, maximum value (kN)	Shear force at fixed end (kN)	$w_{\max}$ (mm)	F_{pri}, (kN)	F_{pro}, (kN)
0.00	2.0380	− 10.2134	− 1.0956	0.9904	6.3918	15.9290
0.20	2.0380	− 10.2134	− 1.1445	1.0743	6.9398	17.3638
0.40	2.0380	− 10.2134	− 1.2332	1.1715	7.6077	19.0395
0.60	2.1282	− 10.2134	− 1.3502	1.2781	8.3605	20.8850

Table 5. Comparison of calculation results for building structure configuration contraction scenarios.

Variables	Values
l_{ppi}	$0.80l_{\mathrm{ni}}$, $0.85l_{\mathrm{ni}}$, $0.90l_{\mathrm{ni}}$, $0.95l_{\mathrm{ni}}$, $1.00l_{\mathrm{ni}}$
l_{ppo}	$0.80l_{\mathrm{no}}$, $0.85l_{\mathrm{no}}$, $0.90l_{\mathrm{no}}$, $0.95l_{\mathrm{no}}$, $1.00l_{\mathrm{no}}$
I-beam specifications	I14, I16, I18, I20a
Inner tie rod diameter d_{pri} (mm)	0, 18, 20, 22, 24
Outer tie rod diameter d_{pro} (mm)	0, 18, 20, 22, 24

Table 6. Values of variables.

along the length of the main beam at various cross-sections, and V_{z} represents the maximum shear force along the length of the main beam at various cross-sections. As shown in the table, with the increase in the vertical force F_{n} transmitted by the uprights, the internal forces of the main beam, deflection of the main beam, and tension rod forces all increase significantly. The shear force at the fixed end of the main beam also increases substantially, roughly equivalent to the increase in F_{n}. It is recommended that regular inspections be conducted during the actual use of the scaffolding to ensure the integrity of the bolts at the connection points between the main beam and the building structure, as well as the connection nodes between the uprights and the main beam, to ensure the smooth operation of the main beam and the proper transfer of loads by the uprights.

(4) Contraction of building structure configuration

The contraction of building structure configuration, denoted as $l_0 \neq 0$, is investigated by considering four scenarios with l_0 taken as 0.00 *h*, 0.20 *h*, 0.40 *h*, and 0.60 *h* respectively, as shown in Table 5. As the contraction of the building structure configuration increases, there is minimal variation in the internal forces of the main beam itself. However, the shear force at the fixed end nodes of the main beam, maximum deflection, and tension rod axial force all increase. It is recommended that in practical design work, the sections of tension rods may be enlarged in areas where the building structure configuration contracts.

Multivariable computational analysis

Both the positions of the tension rod and the connection node on the main beam, denoted as l_{ppi} and l_{ppo} respectively, have an impact on the structural performance of the cantilevered steel truss scaffolding. Additionally, the specifications of the I-beam used for the cantilevered main beam and the tension rod will also influence the structural performance of the scaffolding. To elucidate the effects of these variables on the structural performance, a single-factor variable method was employed for analysis. The variables used in the analysis and their respective values are presented in Table 6. Apart from the variables subject to change, the remaining variables were set to the values indicated in Table 2.

Analysis of influencing factor l_{ppi}

Under different positions for the connection point of the inner tie rod and the main beam, the internal force calculation of the main beam is shown in Table 7. From the table, it can be observed that as the connection point moves away from the fixed end of the main beam, the internal forces of the main beam remain essentially unchanged, while the deflection gradually decreases slightly. This is mainly because, with both tie rods present, the effect of the outer tie rod is much greater than that of the inner tie rod. Therefore, adjusting the position of the inner tie rod connection point does not have a significant impact on the stress and deformation of the main beam when the outer tie rod is present. Where feasible, it is recommended to consider positioning the inner tie rod connection point with the main beam as close to the inner support position as possible.

l_{ppi}/l_{ni}	M_y, maximum value (kN m)	V_z, maximum value (kN)	w_{max} (mm)	l_{ppo}/l_{no}	M_y, maximum value (kN·m)	V_z, maximum value (kN)	w_{max} (mm)
0.80	2.0379	− 10.213	1.0155	0.80	4.0847	− 10.263	1.6159
0.85	2.0380	− 10.213	1.0040	0.85	3.0567	− 10.238	1.2616
0.90	2.0380	− 10.213	0.9904	0.90	2.0380	− 10.213	0.9904
0.95	2.0381	− 10.213	0.9745	0.95	1.9685	− 10.189	0.7954
1.00	2.0383	− 10.213	0.9561	1.00	2.2569	− 8.9566	0.6688

Table 7. Comparison of calculation results of different pull rod and main beam tie point positions.

Specifications of the main beam	M_y, maximum value (kN m)	V_z, maximum value (kN)	Shear force at the fixed end (kN)	w_{max} (mm)	F_{pri} (kN)	F_{pro} (kN)
I14	2.0360	− 10.2004	− 0.7034	1.0492	6.4415	16.2251
I16	2.0380	− 10.2134	− 1.0956	0.9904	6.3918	15.9290
I18	2.3835	− 10.2264	− 1.5837	0.9470	6.2947	15.5736
I20a	3.3283	− 10.2399	− 2.2088	0.9062	6.1443	15.1216

Table 8. Comparison of calculation results of different I-beam specifications of main beam.

d_{pri} (mm)	M_y, Maximum value (kN m)	F_{pro}(kN)	w_{max}(mm)	d_{pro}(mm)	M_y, Maximum value (kN m)	F_{pro}(kN)	w_{max}(mm)
0.00	3.8025	18.582	1.0555	0.00	3.4539	0.0000	6.3629
18.00	1.9100	16.256	0.9985	18.00	1.7070	15.372	1.1784
20.00	1.6437	15.929	0.9904	20.00	1.6437	15.929	0.9904
22.00	1.3929	15.621	0.9829	22.00	1.5938	16.368	0.8424
24.00	1.1593	15.334	0.9758	24.00	1.5540	16.718	0.7242

Table 9. Comparison of calculated results for different tie rod diameters.

Analysis of influencing factor l_{ppo}

When the attachment position of the outer tie rod to the main beam varies, the computed internal forces of the main beam are likewise presented in Table 7. As shown in the table, as the attachment point of the tie rod moves away from the fixed end of the main beam, both the internal forces and deflections of the main beam gradually decrease. Moreover, the magnitude of this decrease is greater compared to when there are variations in the positions of the inner tie rod relative to the main beam. This is attributed to the greater restraining effect exerted by the outer tie rod compared to the inner tie rod. It is recommended to position the tie rods as close as possible to the adjacent upright positions during engineering design and installation work.

Analysis of the impact of main beam I-Beam specifications

The influence of main beam I-beam specifications on the internal forces of the main beam, main beam deflection, and tie rod internal forces is presented in Table 8. As the dimensions of the main beam I-beam specifications gradually increase, the internal forces increase gradually, while the deflection decreases gradually. The effects of the two tie rods gradually weaken, i.e., the axial force in the tie rods decreases gradually. It is suggested that, in practical design work, if effective control of deflection is required, consideration can be given to increasing the main beam I-beam specifications. Similarly, if it is inconvenient to install tie rods in certain structural parts of a building, consideration can also be given to increasing the main beam I-beam specifications.

Analysis of influencing factor d_{pri}

The influence of the diameter d_{pri} of the tie rod on the internal forces of the main beam, the deflection of the main beam, and the internal forces of the tie rod is shown in Table 9. As the diameter of the tie rod increases, it can be observed from the table that the bending moment of the main beam, the deflection of the main beam, and the tension in the outer tie rod gradually decrease. This is because with the increase in the diameter of the tie rod, its restraining capability on the main beam enhances, consequently reducing the restraining effect of the outer tie rod on the main beam. As a result, both the deflection of the main beam and the tension in the outer tie rod gradually decrease.

Analysis of influencing factor d_{pro}

The influence of the outer tie rod diameter d_{pro} on the internal forces of the main beam, the deflection of the main beam, and the internal forces of the tie rod is also listed in Table 9. From the table, it can be observed that with an increase in the outer tie rod diameter, both the bending moment and deflection of the main beam gradually decrease. Furthermore, the reduction in deflection is greater than the corresponding reduction observed with an increase in the inner tie rod diameter, while the reduction in bending moment is less than the corresponding reduction observed with an increase in the inner tie rod diameter.

Upon examining the computational results in Table 9, when the inner tie rod diameter is zero, indicating only the outer tie rod is in action, the maximum bending moment of the main beam is 3.8025 kN m, and the maximum deflection of the main beam is 1.0555 mm. Conversely, when the outer tie rod diameter is zero, indicating only the inner tie rod is in action, the maximum bending moment of the main beam is 3.4539 kN m, and the maximum deflection of the main beam is 6.3629 mm. A comparison reveals that the sole action of the outer tie rod exceeds that of the inner tie rod, suggesting a stronger influence of the outer tie rod. It is recommended for subsequent design work to consider increasing the specification of the outer tie rod while moderately reducing the specification of the inner tie rod. The specifications of the inner and outer tie rods do not necessarily need to be identical. In situations where only a single tie rod can be installed due to constraints, it is advised that the outer tie rod be prioritized. Moreover, for practical construction use, regular inspections of the tie rods, especially the outer tie rod, are recommended to ensure their effectiveness.

Field in-situ testing and finite element verification

Overview of in-situ testing

In order to validate the rationality of the overall stress analysis mentioned above and to quantitatively analyze the safety margin of the structural system composed of the tie rods and main beam in actual construction sites, an experimental system was established at the construction site, as shown in Fig. 7a. This system mainly includes a digital display hydraulic jack loading system (as depicted in Fig. 7b), strain monitoring of the upper flange of the main beam at the wall end (as illustrated in Fig. 7c), and deflection monitoring of the lower flange of the main beam (as shown in Fig. 7d).

In the specific experiment, a 1.4 m long No. 18 I-beam was used as the main beam, with tie rods of 22 mm diameter. The distance between the tie rod connection points and the fixed end of the main beam was 105 cm. During the experiment, three deflection monitoring points were set at the ends and middle of the main beam, with distances from the fixed end of the main beam of 20.5 cm, 71.0 cm, and 119.0 cm, respectively. The axial strain monitoring point of the upper flange of the main beam was located at the fixed end of the main beam.

The two loading points of the experiment were located at distances of 38.0 cm and 118.0 cm from the fixed end of the main beam, respectively. The experiment aimed to simulate the actual construction process as closely as possible, with equal concentrated forces applied at both internal and external loading points. A staged loading pattern was employed, sequentially applying loads of 5.0 kN, 10.0 kN, 15.0 kN, 20.0 kN, 25.0 kN, and 30.0 kN. To ensure simultaneous loading of the main beam and tie rods during subsequent loading processes, the tie rods need to be pre-tensioned before loading begins. The magnitude of the pre-tensioning force should be determined based on the onset of upward deflection at the ends of the main beam. As shown in Fig. 7e, three deflection data points and one strain data point were recorded after each load stage stabilization.

Experimental results analysis

The experimental results obtained under each load level are presented in Table 10. The normal stress in the table is calculated based on the measured strain data. It is evident from the data in the table that as the loads increase in arithmetic progression, the deflections at the internal point, midpoint, and external point, as well as the normal stress, all increase in arithmetic progression. This directly indicates that the system composed of the main beam and tie rods remained in a state of linear elastic behavior throughout the loading process.

Finite element analysis

Finite element analysis is a highly important modern numerical computation method widely applied in engineering practice[35]. In comparison to in-situ experiments, it offers advantages such as lower implementation costs, comprehensive information acquisition, and ease of conducting multivariable analyses[36,37]. The finite element analysis method created by a self-written program was employed to analyze the stress on the tie rods and main beam structural system, with geometric dimensions, loading procedures, displacement monitoring points, and stress monitoring points consistent with the in-situ experiment. After the element discretization is completed, the Newton Simpson iteration method is used to solve the corresponding nonlinear equation system.

Specifically, in the finite element analysis, one end of the main beam was fully fixed while the other end was free, utilizing 2-node linear beam elements. Hinge mode was applied to the nodes on the tie rods, and 2-node linear three-dimensional rod elements were used for the tie rods. Both the main beam and tie rods were made of ordinary carbon steel and were modeled using an ideal elastic-plastic constitutive model, with an elastic modulus of 206 GPa, Poisson's ratio of 0.30, and yield stress of 235 MPa. The computed results are presented in Table 11.

Comparison of three methods

In addition to employing on-site in-situ testing methods and finite element analysis, the internal force calculation formulas presented in Sect. 3 of this paper can also be utilized to easily derive deflections and stresses from the obtained internal force distribution. A comparison of the results obtained from on-site in-situ testing methods, finite element analysis, and analytical methods is shown in Fig. 8. It can be observed from the graph that, apart from the deflection at the internal point, the results obtained by the finite element method and analytical method are very close for the deflections at the midpoint, external point, and normal stress. The curve of the results obtained from on-site testing is generally close to the curves of the results obtained from the finite element method and analytical method. This directly indicates that the relevant calculation formulas derived in this paper are reliable.

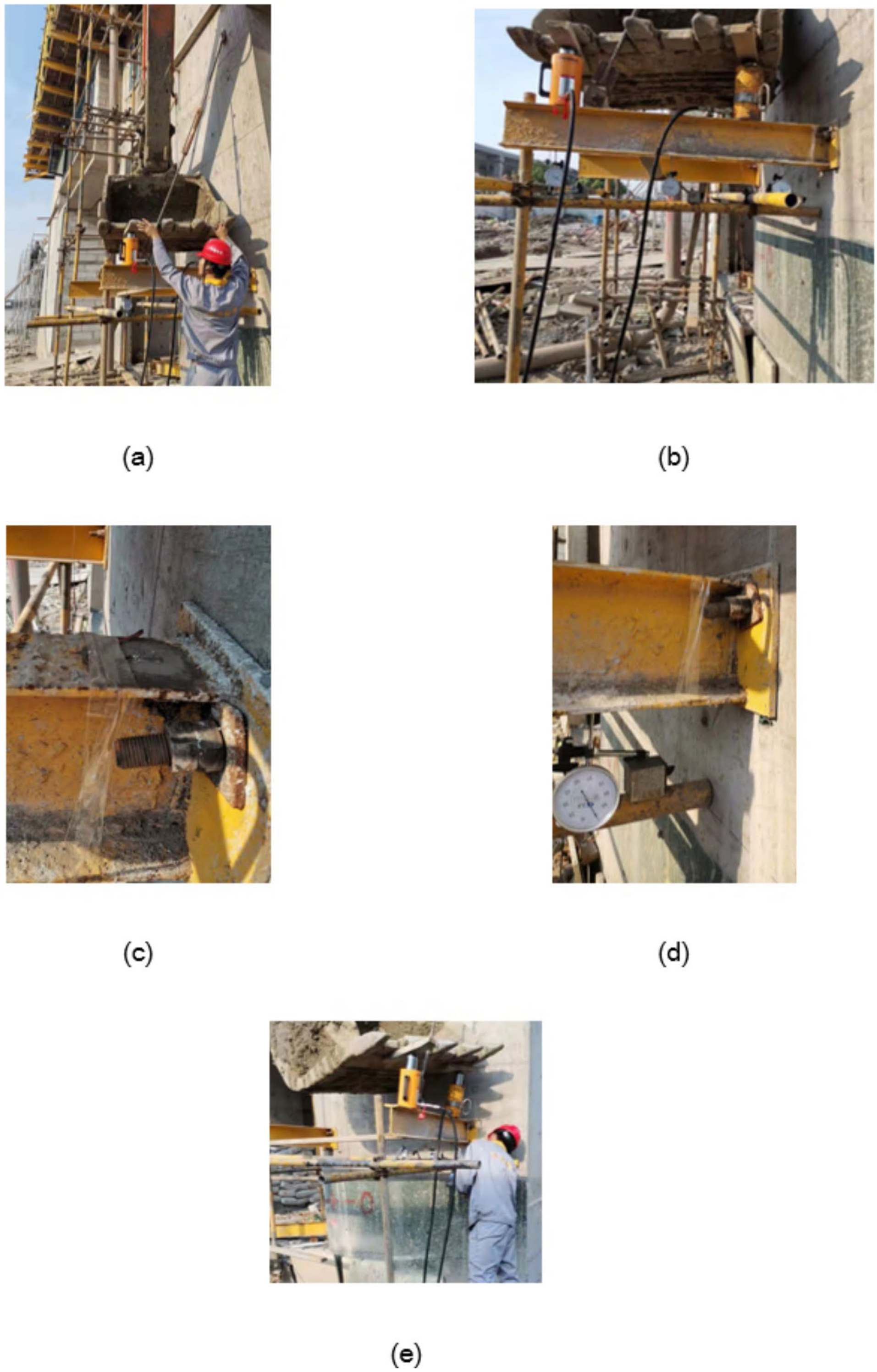

Fig. 7. In situ test: (**a**) integrated test system; (**b**) jack loading; (**c**) strain monitoring of main beam; (**d**) deflection monitoring of main beam; (**e**) test data record.

Analysis of forces on the joints of inclined steel cantilever scaffolding

As shown in Fig. 2b–e, the four major joints of the inclined steel cantilever scaffolding include the joint connecting the main beam to the building structure, the joint connecting the tie rod to the main beam, the upper and lower joint of the tie rod, and the joint connecting the tie rod to the building structure. Ensuring the safety of these four major joints is crucial to guarantee the overall safety of the inclined steel cantilever scaffolding.

Load (kN)	5.0	10.0	15.0	20.0	25.0	30.0
Internal point deflection (mm)	0.0395	0.0533	0.0667	0.0804	0.0939	0.1071
Midpoint deflection (mm)	0.1733	0.2825	0.4014	0.5099	0.6167	0.7269
External point deflection (mm)	0.3413	0.5867	0.8335	1.0781	1.3241	1.5747
Normal stress (kPa)	14.0688	27.3097	40.5505	53.7914	67.0317	80.2731

Table 10. Test results.

Load (kN)	5.0	10.0	15.0	20.0	25.0	30.0
Internal point deflection (mm)	0.0246	0.0483	0.0720	0.0957	0.1194	0.1431
Midpoint deflection (mm)	0.1360	0.2671	0.3981	0.5291	0.6600	0.7911
External point deflection (mm)	0.2875	0.5655	0.8435	1.1215	1.3994	1.6774
Normal stress (kPa)	13.9961	27.4795	40.9628	54.4461	67.9295	81.4129

Table 11. Results of finite element calculation.

Connection node of main beam to building structure

As shown in Fig. 9a, the cantilever main beam is welded to the end plate, while the end plate is connected to the building structure using two bolts. To enhance the connection strength and stability, a triangular gusset plate is added to the flange side of the main beam, which is welded to both the end plate and the main beam. As depicted in Fig. 9b, the weld is a perimeter fillet weld, with continuous welding at the corners. Clearly, this node primarily requires verification of both weld joint and bolted connections.

Welded joint verification

A double-sided fillet weld is used between the cantilever main beam and the end plate. The weld joint is subjected to both pressure and shear forces and needs to be verified using the strength calculation formula specified in the relevant code[34].

Bolted joint verification

Two bolts between the end plate and the building structure are subjected to combined tensile and shear forces. It can be reasonably assumed that each bolt bears equal pressure and shear forces transmitted from the main beam. Verification of the shear bearing capacity of ordinary bolts should be carried out according to the formula specified in the relevant code[34].

Tie rod and main beam connection node

As shown in Fig. 10a, the main beam is welded to the ear plate, as shown in Fig. 2c, the ear plate is connected to the connection plate by bolts, and as shown in Fig. 10b, the connection plate is welded to the lower tie rod. Under these connection conditions, the loads borne by the main beam can be effectively transferred to the tie rod. Clearly, both weld and bolt connection calculations are required for this node.

Welded joint strength calculation

For the right-angled fillet weld between the main beam and the ear plate, which is subjected to both tension and shear forces, it is necessary to calculate the strength of the right-angled fillet weld according to the formula specified in the relevant code[34].

The weld between the connection plate and the lower tie rod primarily experiences shear forces and can be calculated using the formula specified in the relevant code[34] for fillet welds within circular or slotted holes.

Bolted connection calculation

The bolts between the ear plate and the connection plate are subjected to shear forces and should be calculated using the formula for the shear bearing capacity of ordinary bolts specified in the relevant code[34].

Ear plate strength calculation

The ear plate undergoes combined tensile and shear forces and should be calculated using the formula specified in the relevant code[34] for the tensile and shear resistance capacity of the plate at the connection node under tension and shear actions.

Connection nodes at the upper and lower ends of the tie rod

As shown in Figs. 2d and 11, the force on the tie rod is transmitted to the nut through the bolt, and then transferred to three round bars through welding. Therefore, this node requires weld connection, bolt connection, and tensile strength calculation of the three round bars.

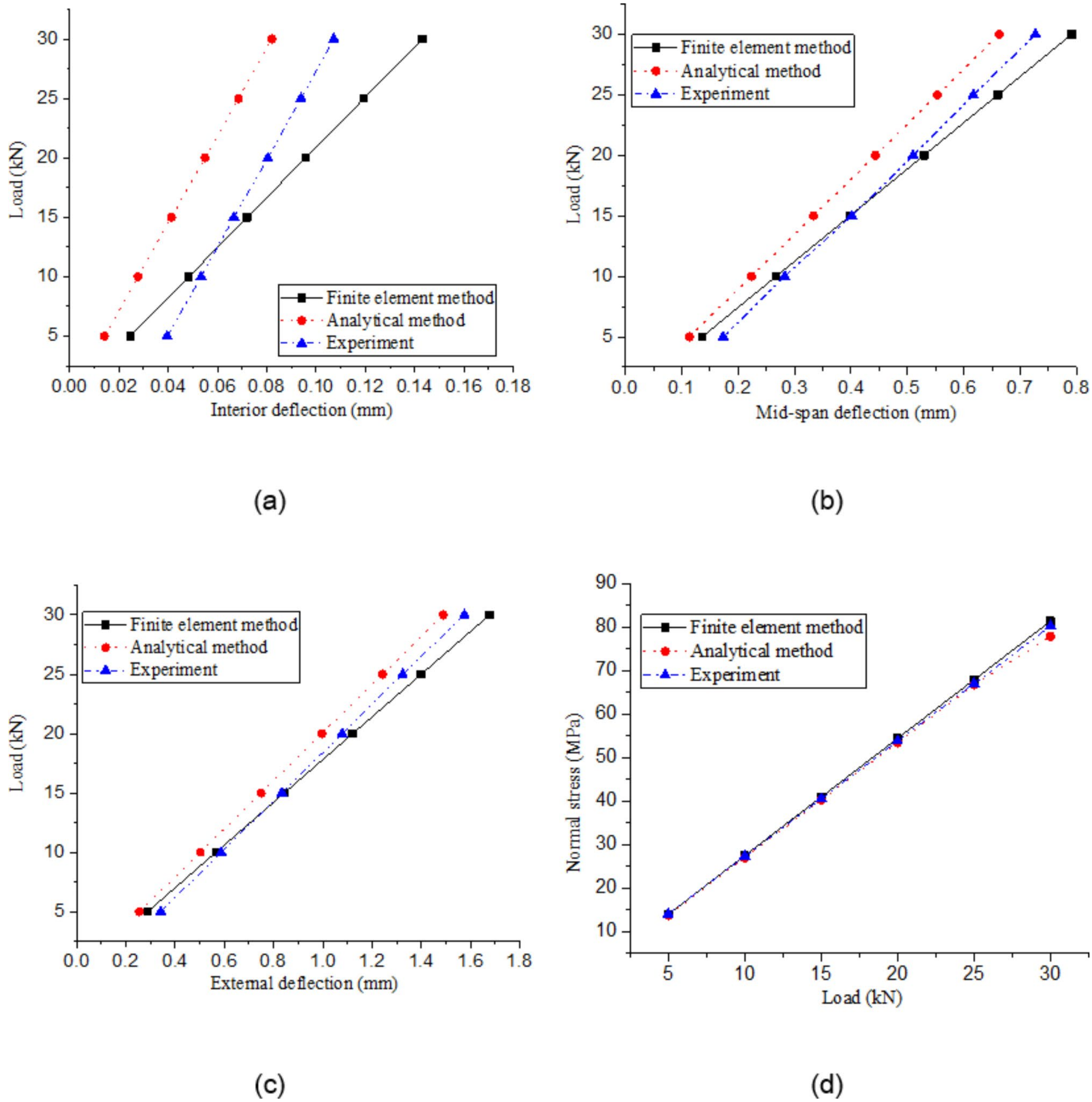

Fig. 8. Comparison of the results of three methods: (**a**) internal point deflection; (**b**) midpoint deflection; (**c**) external point deflection; (**d**) normal stress.

Welded joint strength calculation

The weld between the nut and three round bars mainly withstands shear forces, and the strength of the fillet weld parallel to the length of the weld can be calculated according to the formula specified in the relevant code[34].

Bolted connection calculation

The bolt composed of the nut and tie rod bears axial tensile forces, and the bearing capacity of the axial tensile ordinary bolt can be calculated according to the formula specified in the relevant code[34].

Tensile strength calculation of three round bars

It can be reasonably assumed that each of the three round bars bears one-third of the tension force of the tie rod, and the round bars can be strength-calculated as axial tension members.

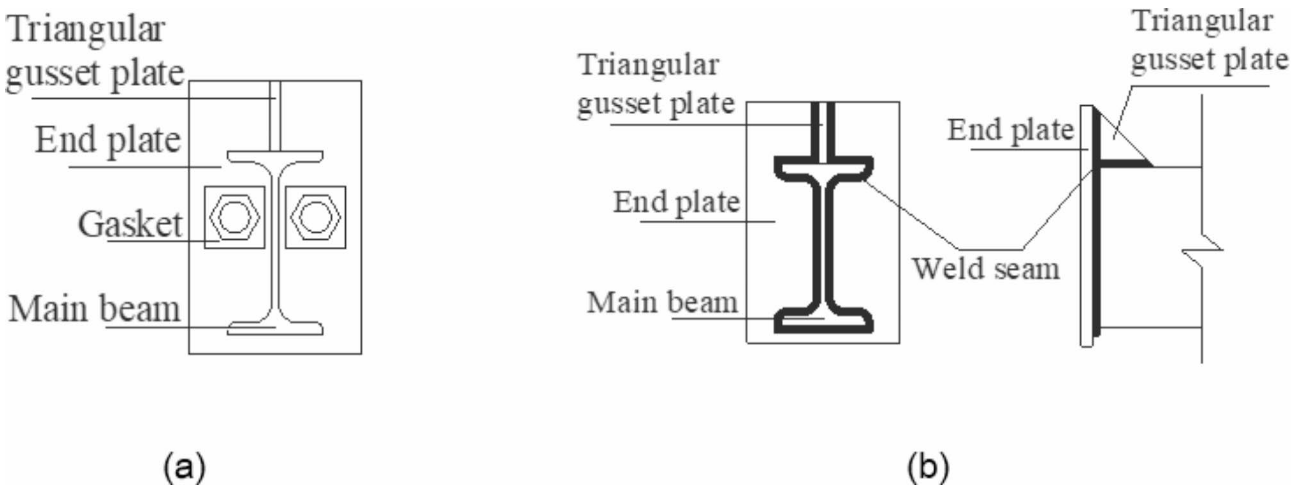

Fig. 9. Connection node of main beam to building structure: (**a**) node section; (**b**) welding.

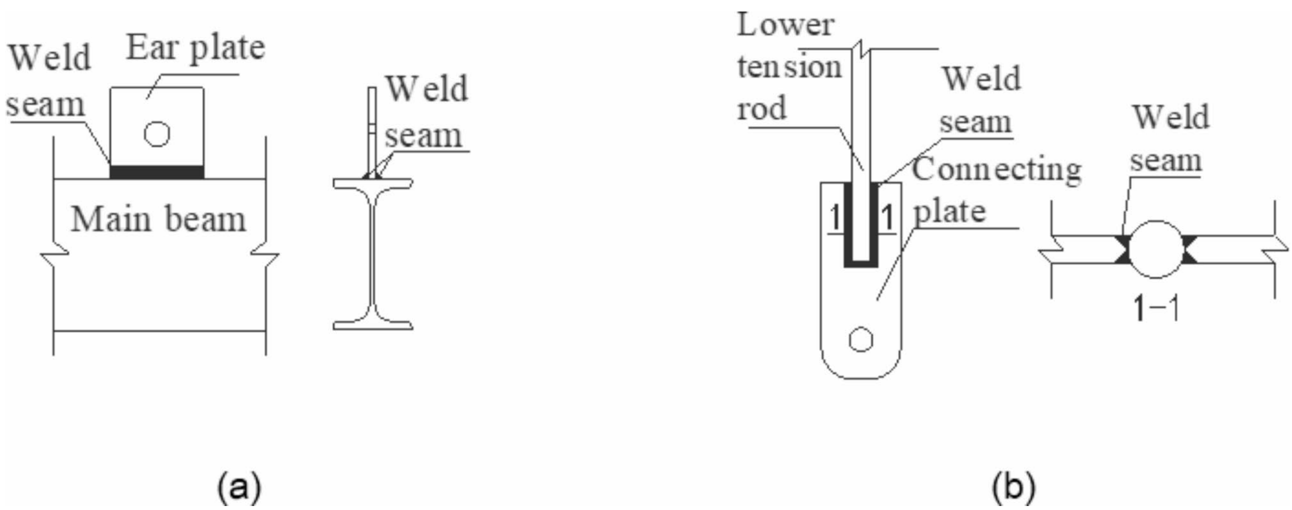

Fig. 10. Connection node of tie rod and main beam: (**a**) welding between ear plate and main beam; (**b**) welding between connection plate and lower tie rod.

Connection node of tie rod and building structure
From Figs. 2e and 12, it can be observed that the top tension rod is connected to the end plate through welding, while the end plate is connected to the building structure through bolts. Clearly, both weld and bolt connection calculations are required for this node.

Weld connection calculation

The weld between the end plate and the top tension rod primarily experiences shear forces and shall be calculated using the fillet weld calculation formula specified in the relevant code[34] for circular or slotted hole.

Bolt connection calculation

The bolts between the end plate and the building structure are subjected to combined tensile and shear actions. The strength of ordinary bolts under simultaneous shear and axial tensile forces, as specified in the relevant code[34], shall be calculated using the appropriate strength calculation formula.

To facilitate the calculation of the four major nodes in the design of the inclined steel cantilever scaffolding, the summary of the calculations required for the four nodes is presented in Table 12.

Design process and application
Design process
Based on the research findings above and in conjunction with relevant design codes for cantilever scaffolding[34], the design process for the inclined-type steel cantilever scaffolding as shown in Fig. 13 can be derived. Initially, the design parameters for the inclined-type steel cantilever scaffolding are preliminarily determined, followed by

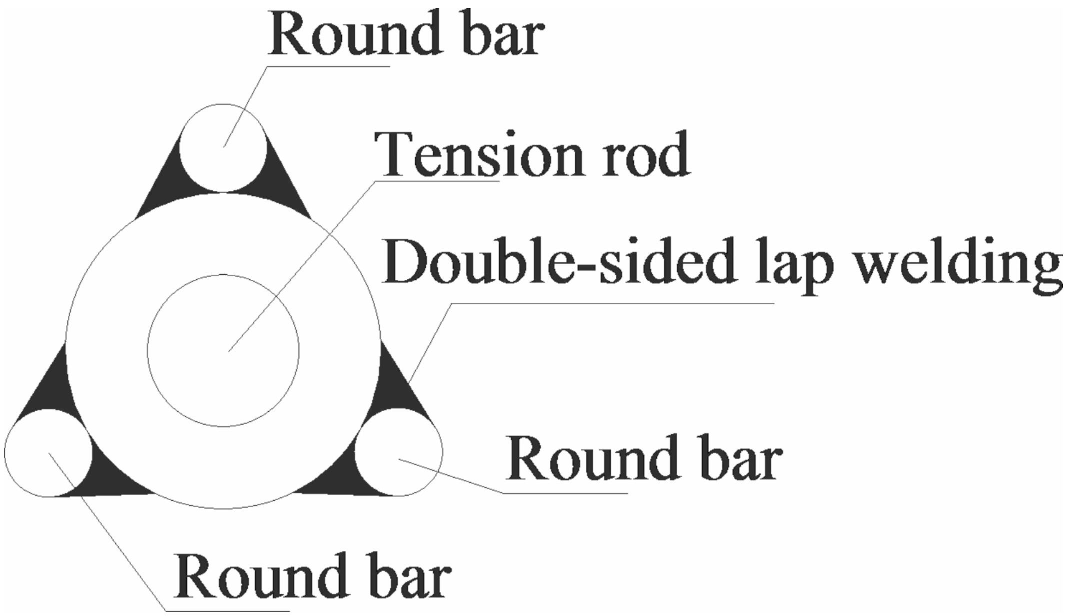

Fig. 11. Connection nodes at the upper and lower ends of the tie rod.

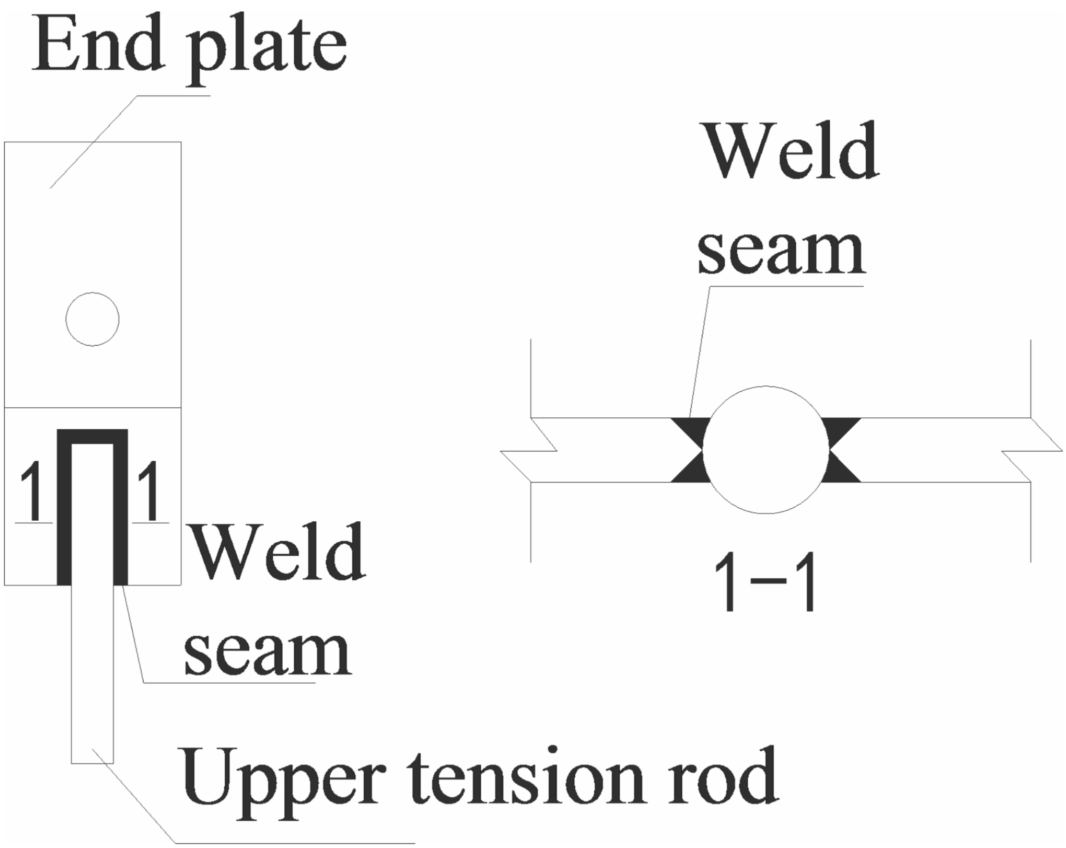

Fig. 12. Connection node of tie rod and building structure.

establishing the external loads on the scaffolding in accordance with the relevant codes[34], i.e., determining the design value of the concentrated load as F_n. Subsequently, the overall structural analysis of the inclined-type steel cantilever scaffolding is carried out according to Eqs. (1)–(16), including the full-process design calculations as presented in Table 1 and the design verification for special conditions as shown in Table 3. Upon satisfying the requirements for strength, deformation, and stability in both the full-process design calculations and the design

Node locations	Welded joint verification	Bolted joint verification	Strength verification
Connection node between main beam and building structure	Weld seam between main beam and end plate, strength calculation of right-angle fillet welds.	Bolts between end plate and building structure, calculation of shear bearing capacity of ordinary bolts.	–
Connection node between tie rod and main beam	Weld seam between main beam and ear plate, strength calculation of right-angle fillet welds Weld seam between connection plate and lower tie rod, calculation of fillet welds in circular or slotted holes.	Bolts between ear plate and connection plate, calculation of shear bearing capacity of standard bolts.	Ear plate, calculation of tensile fracture bearing capacity under tensile-shear action
Upper and lower connection nodes of tie rods.	Weld between nut and three round bars, strength calculation of side fillet welds.	Bolt composed of nut and tie rod, calculation of bearing capacity for axially loaded ordinary bolts.	Three round bars, axial tensile strength calculation.
Connection node of tie rod with the building structure	Weld between end plate and upper tie rod, calculation of fillet weld in circular or slotted holes.	Bolts between end plate and building structure, strength calculation of ordinary bolts under tensile-shear action.	–

Table 12. Joints checking summary.

verification for special conditions, the strength verification for the four major nodes is conducted as per Table 12. Once the strength verification for the four major nodes also meets the requirements, the design parameters for the inclined-type steel cantilever scaffolding can be finalized. If not, adjustments to the parameters are necessary, and the design process, as illustrated in Fig. 13, is reiterated until both the full-process design calculations and the design verification for special conditions meet the strength, deformation, and stability requirements, with the strength of the four major nodes meeting the specified criteria.

Engineering application

The inclined steel cantilever scaffolding was utilized in the real estate development project at Plot no. 2017G72 in Nanjing, with a focus on the inclined steel cantilever scaffolding for Building 4 # as an example. The scaffolding was initially planned for 4 stages of cantilevering, with specific parameters detailed in Table 13. Following the design process illustrated in Fig. 13 leads to the design of the inclined steel cantilever scaffolding for Building 4 #, as shown in Fig. 14. Upon completion of the design, a tally of the steel profiles and tie rods used was conducted, with the results presented in Table 14.

The cost of the inclined steel cantilever scaffolding system mainly includes main beams, tension rods, bolt connectors, technical services, inspection fees, labor costs, etc. On the other hand, the cost of the fully cantilevered scaffolding system mainly comprises main beams, unloading ropes, U-shaped rings, technical services, inspection fees, labor costs, etc. To conduct a comparative economic analysis of the two scaffolding systems, the main beams of the fully cantilevered support system were selected to ensure that the deflection and maximum principal stress of the corresponding main beams were similar to those of the inclined steel cantilever scaffolding system. The resulting costs for the fully cantilevered scaffolding system and the inclined steel cantilever scaffolding system were determined to be 83,454 yuan and 42,617 yuan, respectively. Compared to the fully cantilevered scaffolding system, the inclined steel cantilever scaffolding system can save 48.93% of the cost. This is primarily due to the fact that the main beams of the fully cantilevered scaffolding system cannot fully bear loads directly within the building structure, and these main beams are fully cantilevered components with significant material utilization efficiency variances along the length of the main beam.

Based on on-site observations, the dismantling period for the inclined steel cantilever scaffolding system is 1.5 days, whereas for the fully cantilevered scaffolding system, it is 4.0 days. The dismantling period for the inclined steel cantilever scaffolding system is only 37.5% of that for the fully cantilevered scaffolding system, indicating significantly higher construction efficiency. This is primarily attributed to the inclined steel cantilever scaffolding system's use of bolt connections, which facilitate fast installation and dismantling. The small openings left on the building structure only require grouting for sealing, leading to enhanced construction efficiency. In contrast, during the dismantling of fully cantilevered scaffolding systems, cutting of U-shaped rings is often necessary, and the larger openings left behind typically require concrete or block sealing, resulting in longer construction durations.

Compared to fully cantilevered scaffolding systems, the inclined steel cantilever scaffolding features shorter main beam lengths, smaller cross-sectional areas, and lighter weights, resulting in lower labor intensity and higher construction efficiency for workers during operations. The inclined steel cantilever scaffolding demonstrates higher material utilization efficiency, aligning with the policy demands for conserving resources and energy. Furthermore, the system primarily involves cold operations, meeting the policy-oriented requirements for safe and civilized construction practices. In contrast, fully cantilevered scaffolding systems have larger openings in their structures, posing challenges for sealing and significantly increasing the risk of wall leakage, directly impacting the occupants' living experience and raising maintenance costs in the future.

Conclusions

In order to reduce the cost of scaffolding in engineering projects while ensuring safety and avoiding leakage risks caused by holes reserved for scaffolding on building structures, a theory-based analysis method was proposed to develop an inclined steel cantilever scaffolding system, considering the structural characteristics of traditional cantilever scaffolding. Through a comprehensive approach involving theoretical analysis, on-site tests, and finite element methods, a clear full-process design methodology for the inclined steel cantilever scaffolding was established, providing recommendations for practical engineering design and application of this system. The

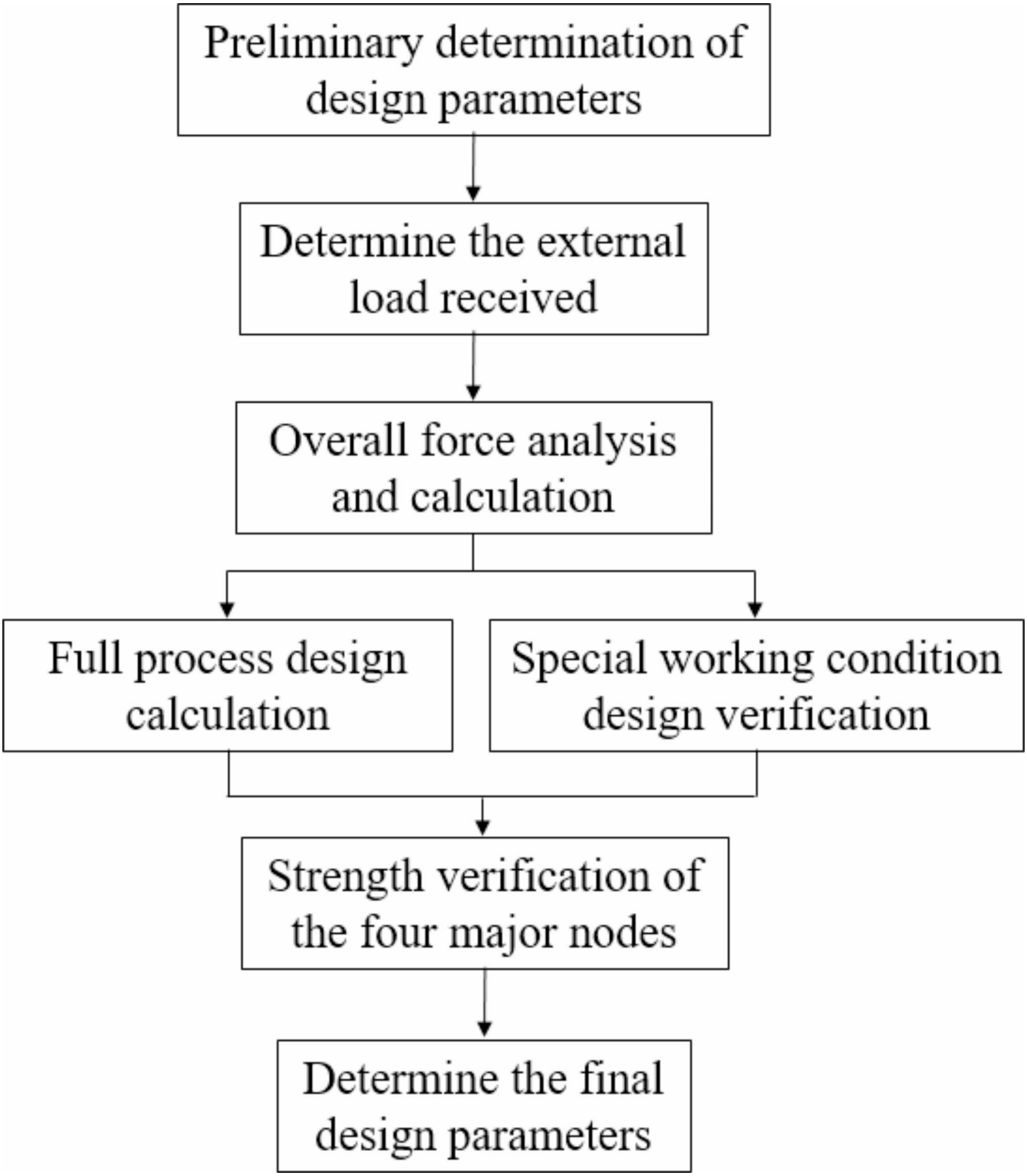

Fig. 13. Design process.

inclined steel cantilever scaffolding was successfully applied in actual engineering projects. The research findings indicate:

(1) The calculated formulas for internal forces in the main beam and tie rods of the inclined steel cantilever scaffolding are feasible and can serve as references in specific design tasks. It is noted that the dismantling process poses more adverse loading conditions compared to the installation process, necessitating thorough calculations during dismantling.
(2) Offset of nodes on the tie rods adversely affects the loading on the main beam and fixed joints. It is recommended to avoid tie rod offsets or establish two sets of tie rod systems symmetrically with respect to the

Building number	Number of floors	Floor height (m)	Scaffolding system	Starting floor/elevation	Ending floor/elevation	Scaffolding height (m)	Number of scaffolding floors
4#	25	3	Inclined tensioned steel cantilevered scaffolding	4 F (bottom)/8.9 m	10 F (bottom)/26.9 m	18	6
				10 F (bottom)/26.9 m	16 F (bottom)/44.9 m	18	6
				16 F (bottom)/44.9 m	22 F (bottom)/62.9 m	18	6
				22 F (bottom)/66.9 m	equipment room floor + 1.2 m/81.2 m	14.3	6

Table 13. Preliminary design of the layered inclined steel cantilever scaffolding system for the building No. 4.

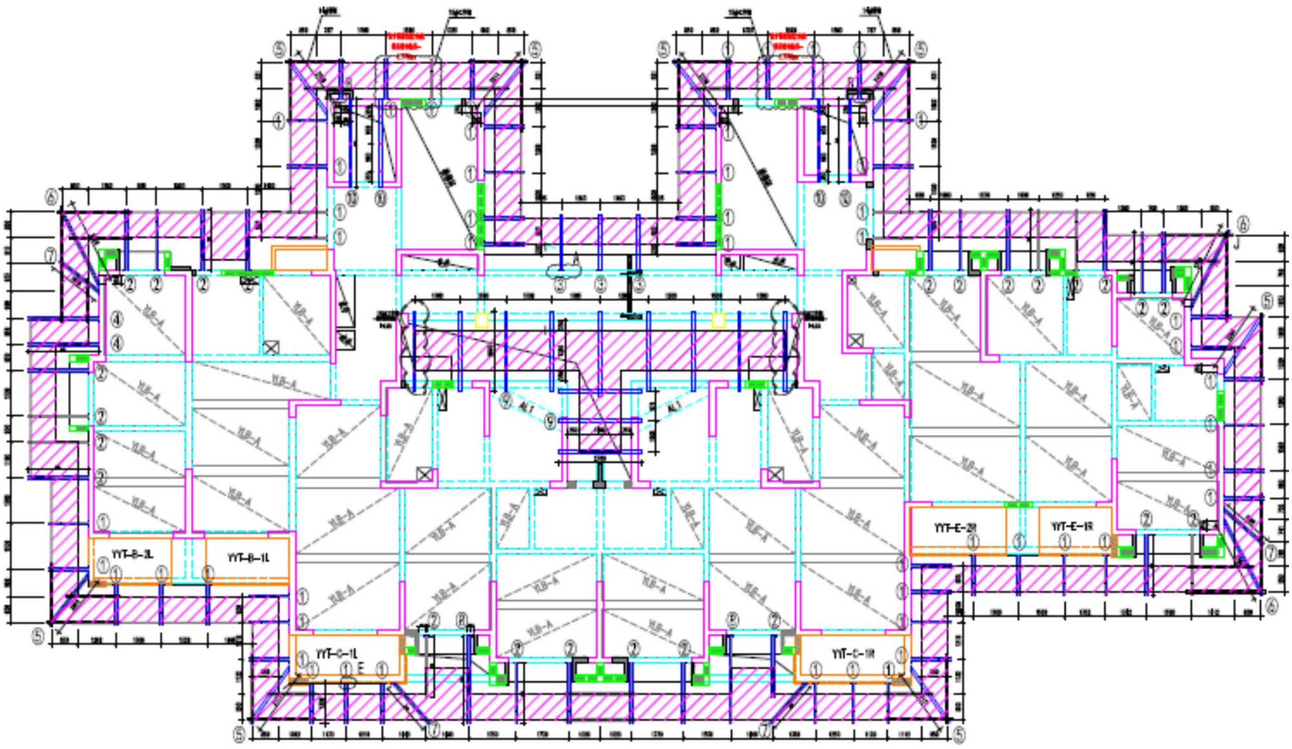

Fig. 14. Plan positioning diagram of cantilever steel.

Number	Steel type	Steel length (m)	Quantity	Corresponding tension rod and specification
1	I 18	1.30	52	Single pull rod $d = 2$ cm
2	I 18	1.99	24	Single pull rod $d = 2$ cm
3	I 18	1.79	3	Single pull rod $d = 2$ cm
4	I 18	2.34	2	Single pull rod $d = 2$ cm
5	I 18	2.20	8	Double pull rod $d_{pri} = d_{pro} = 2$ cm
6	I 18	2.70	15	Double pull rod $d_{pri} = d_{pro} = 2$ cm
7	I 18	1.70	4	Double pull rod $d_{pri} = d_{pro} = 2$ cm
8	I 18	2.80	2	Double pull rod $d_{pri} = d_{pro} = 2$ cm
9	I 18	2.90	4	Double pull rod $d_{pri} = d_{pro} = 2$ cm

Table 14. Statistical table of steel shapes and tie rods.

vertical plane of the main beam. In the presence of outer tie rods, the effectiveness of internal tie rods is limited. When both tie rods fail completely, the bending moment of the main beam increases to 16 times that when neither is failed. It is advised to have outer tie rods in place and conduct regular inspections on tie rods, especially the outer ones, to ensure their functionality.

(3) Internal forces and displacements in the main beam and tie rods increase proportionally with the vertical force transmitted by the vertical posts. Regular inspections on bolts at the connection points between the main beam and building structure, as well as the connection points between vertical posts and the main beam, are recommended to ensure the proper functioning of the main beam and the smooth transfer of loads by the vertical posts.
(4) Under conditions where the deflection at the end of the main beam is the same and the maximum principal stress in the main beam is equal, the inclined steel cantilever scaffolding system saves 48.93% in costs and 62.5% in construction time compared to a fully cantilevered scaffolding system. Additionally, it offers significant social benefits, suggesting its potential for widespread adoption in engineering practices.

The design methodology proposed for the inclined steel cantilever scaffolding system can be promoted in engineering design work. However, given the decreasing profitability in engineering projects, optimizing scaffold design becomes crucial. While this study did not delve into this aspect, it is recommended for future research to employ optimization theories based on the findings of this study to optimize the design of the inclined steel cantilever scaffolding system, providing valuable insights for cost reduction and efficiency improvement in the construction industry.

Data availability
Some or all data that support the findings of this study are available from the corresponding author upon reasonable request.

Received: 17 May 2024; Accepted: 17 September 2024
Published online: 13 November 2024

References
1. Weesner, L. B. & Jones, H. L. Experimental and analytical capacity of frame scaffolding. *Eng. Struct.*23 (6), 592–599. https://doi.org/10.1016/S0141-0296(00)00087-0 (2001).
2. Chen, D., Ding, K. & He, X. Force mechanism and progressive collapse of steel tube-coupler scaffold under local load. *KSCE J. Civ. Eng.*22, 2344–2353. https://doi.org/10.1007/s12205-017-1022-y (2018).
3. Wu, L., Zheng, Y., Gao, X. & Wang, Z. Progressive Collapse Resistance of Formwork Support System with couplers. *Math. Modelling Eng. Probl.*7 (3), 403. https://doi.org/10.18280/mmep.070310 (2020).
4. El Sayed, A. Y., Darwish, M. & Nassar, K. Design and constructability of novel extendable arched steel truss falsework. *J. Constr. Eng. Manag.*147 (3), 04020187. https://doi.org/10.1061/(ASCE)CO.1943-7862.0001989 (2021).
5. Martinez, C. J. C., Perea, Y. J. M. N. & Nunez, M. P. Minimum safety criteria in the design stage of supported and suspended scaffolding. In *2022 8th International Engineering, Sciences and Technology Conference (IESTEC)*, pp. 154–161. IEEE. https://doi.org/10.1109/IESTEC54539.2022.00031 (2022).
6. Chandrangsu, T. & Rasmussen, K. J. Investigation of geometric imperfections and joint stiffness of support scaffold systems. *J. Constr. Steel Res.*67, 576–584. https://doi.org/10.1016/j.jcsr.2010.12.004 (2011).
7. Chotickai, P. & Kaewsawang, S. Experimental and analytical studies of door-type modular scaffolds with initial geometrical imperfections. *Eng. J.*22 (6), 135–150. https://doi.org/10.4186/ej.2018.22.6.135 (2018).
8. Tao, D., Nan, X., Zhiting, L. & Feifes, Q. Probabilistic limit state design of falsework considering joint lap defects during concrete pouring period. *J. Southeast. Univ./Dongnan Daxue Xuebao*51(4), 575. https://doi.org/10.3969/j.issn.1001-0505.2021.04.004 (2021).
9. Mercier, C., Khelil, A., Al Mahmoud, F., Blin-Lacroix, J. L. & Pamies, A. Experimental investigations of buckling behaviour of steel scaffolds. *Structures*. 33, 433–450. https://doi.org/10.1016/j.istruc.2021.04.045 (2021).
10. Chandrangsu, T. & Rasmussen, K. J. Structural modelling of support scaffold systems. *J. Constr. Steel Res.*67 (5), 866–875. https://doi.org/10.1016/j.jcsr.2010.12.007 (2011).
11. Li, X., Lam, R. C. Y. & Lam, L. C. H. IoT enabled monitoring scheme for scaffold-frame systems for transfer plate construction. In *International Conference on Smart Transportation and City Engineering (STCE 2022)*, 12460, 730–734. https://doi.org/10.1117/12.2657920 (2022).
12. Wang, F., Tamura, Y. & Yoshida, A. Interference effects of a neighboring building on wind loads on scaffolding. *J. Wind Eng. Ind. Aerodyn.*125, 1–12. https://doi.org/10.1016/j.jweia.2013.11.009 (2014).
13. Wang, S., Sun, Q. & Yang, J. Performance analysis of high steel tube lattice support system in typhoon area. *Stavebni-obzor Civil Eng. J.* 29(2). https://doi.org/10.14311/CEJ.2020.01.0013 (2020).
14. Chan, J. L. & Lo, S. H. Stability design of system scaffold with differential settlement. *Structures*. 27, 1467–1478. https://doi.org/10.1016/j.istruc.2020.07.024 (2020).
15. Wang, Y., Li, T., Dong, K., Guo, Z. & Fu, J. Research on the design safety factor of the supporting falsework considering the installation gaps. *Adv. Civil Eng.* 9262924. https://doi.org/10.1155/2022/9262924 (2022).
16. Jia, L., Liu, H., Chen, Z., Liu, Q. & Wen, S. Mechanical properties of right-angle couplers in steel tube–coupler scaffolds. *J. Constr. Steel Res.*125, 43–60. https://doi.org/10.1016/j.jcsr.2016.06.005 (2016).
17. Andre, J., Beale, R. & Baptista, A. M. Numerical analysis of bridge falsework Cuplok systems. *Proc. Inst. Civ. Eng. Struct. Build.*172(3), 170–188. https://doi.org/10.1680/jstbu.16.00082 (2019).
18. Zhao, Z., Liu, H., Dong, J. & Bian, Y. Buckling capacity of socket-template scaffold system without X-bracing. *J. Perform. Constr. Facil.*34 (1), 04019089. https://doi.org/10.1061/(ASCE)CF.1943-5509.0001373 (2020).
19. Yusuf, B. M. W. M., Abdullah, E. & Mohamed, I. F. Performance of Pre-fabricated Frame Scaffolds Falsework. In *Proceedings of the Sustainable Concrete Materials and Structures in Construction 2020: Towards Sustainable Green Concrete*, pp.215–227. (Springer Singapore, Singapore, 2021). https://doi.org/10.1007/978-981-16-2187-1_19.
20. Abdel-Jaber, M., Abdel-Jaber, M. S., Beale, R., Allouzi, R. & Shatarat, N. Properties of tube and fitting scaffold connections under cyclical loads. *J. Constr. Steel Res.*168, 106008. https://doi.org/10.1016/j.jcsr.2020.106008 (2020).
21. Abdel-Jaber, M. S., Beale, R. G., Godley, M. H. R. & Abdel-Jaber, M. Rotational strength and stiffness of tubular scaffold connectors. *Proc. Inst. Civ. Eng. Struct. Build.* 162(6), 391–403. https://doi.org/10.1680/stbu.2009.162.6.391 (2009).
22. Andre, J., Beale, R. & Baptista, A. M. Experimental analysis of bridge falsework Cuplok systems. Proc. Inst. Civ. Eng. Struct. Build. 171, 719–734. https://doi.org/10.1680/jstbu.16.00081 (2018).
23. Zhang, Y. et al. Research on the bi-directional bending performance of plug-pin scaffold joints in low-temperature. *J. Constr. Steel Res.*213, 108343. https://doi.org/10.1016/j.jcsr.2023.108343 (2024).
24. Bong, J. K. et al. Probabilistic characteristics of moment capacity and rotational stiffness of wedge joints used in support systems reflecting reused members. *Appl. Sci.*9 (19), 4056. https://doi.org/10.3390/app9194056 (2019).

25. Alqattan, H. F., El Aghoury, I. M. & Ibrahim, S. A. B. Numerical evaluation of wedge-type falsework joint. *Asian J. Civil Eng.***25** (2), 1331–1348. https://doi.org/10.1007/s42107-023-00846-4 (2024).
26. Li, Y., Wu, B., Zhang, Y. & Cheng, X. Research on the compressive performance of plug-pin scaffold joints in low-temperature. *J. Constr. Steel Res.***216**, 108497. https://doi.org/10.1016/j.jcsr.2024.108497 (2024).
27. Pienko, M. & Blazik-Borowa, E. Experimental studies of ringlock scaffolding joint. *J. Constr. Steel Res.***173**, 106265. https://doi.org/10.1016/j.jcsr.2020.106265 (2020).
28. Pienko, M. & Blazik-Borowa, E. Numerical analysis of load-bearing capacity of modular scaffolding nodes. *Eng. Struct.***48**, 1–9. https://doi.org/10.1016/j.engstruct.2012.08.028 (2013).
29. Pienko, M. & Blazik-Borowa, E. Verification of the numerical model of insert-type joint of scaffolding in relation to experimental research. In *Proc. AIP Conf. Proc.* (AIP Publishing LLC, 2018). https://doi.org/10.1063/1.5019074.
30. Lam, R. C., Lam, L. C., Li, N. X., Chu, D. L. & Lee, P. K. IoT enabled falsework monitoring system for construction safety enhancement. In 2019 International Conference on Computational Science and Computational Intelligence (CSCI), 1208–1213 (IEEE, 2019). https://doi.org/10.1109/CSCI49370.2019.00227.
31. Lam, R. C. Y., Lam, L. C. H., Li, N. X. & Lee, P. K. K. IoT-based Monitoring System to Prevent Collapse of Falsework Systems During Construction. In 2021 International Conference on Computational Science and Computational Intelligence (CSCI), 1454–1459. IEEE. (2021). https://doi.org/10.1109/CSCI54926.2021.00080.
32. Huang, Y. L. et al. A monitoring method for scaffold-frame shoring systems for elevated concrete formwork. *Comput. Struct.***78** (5), 681–690. https://doi.org/10.1016/S0045-7949(00)00051-1 (2000).
33. Ministry of Housing and Urban-Rural Development of the People's Republic of China. *General Administration of Quality Supervision, Inspection and Quarantine of the People's Republic of China. Unified Technical Standards for Construction Scaffolding Safety GB51210-2016* (China Architecture & Building, 2017).
34. Ministry of Housing and Urban-Rural Development of the People's Republic of China. *General Administration of Quality Supervision, Inspection and Quarantine of the People's Republic of China. Steel Structure Design Standard GB50017-2017* (China Architecture & Building, 2017).
35. Rabi, M., Cashell, K. A. & Shamass, R. J. E. S. Flexural analysis and design of stainless steel reinforced concrete beams. *Eng. Struct.***198**, 109432. https://doi.org/10.1016/j.engstruct.2019.109432 (2019).
36. Rabi, M., Cashell, K. A. & Shamass, R. Ultimate behaviour and serviceability analysis of stainless steel reinforced concrete beams. *Eng. Struct.***248**, 113259. https://doi.org/10.1016/j.engstruct.2021.113259 (2021).
37. Abarkan, I. et al. Machine learning for optimal design of circular hollow section stainless steel stub columns: a comparative analysis with Eurocode 3 predictions. *Eng. Appl. Artif. Intell.***132**, 107952. https://doi.org/10.1016/j.engappai.2024.107952 (2024).

Acknowledgements
The authors are grateful to funding received from the Science and Technology Research Program of Chongqing Municipal Education Commission (No.KJQN202303236) and Project of China Construction 4th Engineering Bureau (No.CSCEC4B-2022-KTA-10, No. CSCEC4B-2023-KTA-10, No.CSCEC4B-2023-KTB-24, No.CSCEC4B-2023-KTB-25, No.CSCEC4B-2023-KTC-23).The financial support is greatly appreciated. In addition, the authors would like to express our gratitude to the workers who worked hard during the on-site experiment in this paper.

Author contributions
Conceptualization, Zhihui Zhao, Dajiang Geng and Xiaohuan Wu; methodology, Yanping Zhang, Minjian Long and Enxin Miao; software, Yanping Zhang, Zhihui Zhao; validation, Dajiang Geng and Minjian Long; investigation, Xiaohuan Wu, Enxin Miao; resources, Yanping Zhang, Dajiang Geng and Enxin Miao; writing—original draft preparation, Dajiang Geng and Minjian Long; writing—review and editing, Zhihui Zhao; visualization, Xiaohuan Wu and Enxin Miao; supervision, Xiaohuan Wu, Zhihui Zhao and Dajiang Geng; project administration, Minjian Long, Yanping Zhang and Enxin Miao. All authors reviewed the manuscript.

Declarations

Competing interests
The authors declare no competing interests.

Ethical approval
This research does not concern experiments involving humans and/or animals and does not require the approval of the ethics committee.

Additional information
Correspondence and requests for materials should be addressed to D.G.

Reprints and permissions information is available at www.nature.com/reprints.

Publisher's note Springer Nature remains neutral with regard to jurisdictional claims in published maps and institutional affiliations.

Open Access This article is licensed under a Creative Commons Attribution-NonCommercial-NoDerivatives 4.0 International License, which permits any non-commercial use, sharing, distribution and reproduction in any medium or format, as long as you give appropriate credit to the original author(s) and the source, provide a link to the Creative Commons licence, and indicate if you modified the licensed material. You do not have permission under this licence to share adapted material derived from this article or parts of it. The images or other third party material in this article are included in the article's Creative Commons licence, unless indicated otherwise in a credit line to the material. If material is not included in the article's Creative Commons licence and your intended use is not permitted by statutory regulation or exceeds the permitted use, you will need to obtain permission directly from the copyright holder. To view a copy of this licence, visit http://creativecommons.org/licenses/by-nc-nd/4.0/.

© The Author(s) 2024